Effective dynamics for low-amplitude transient elastic waves in a 1D periodic array of non-linear interfaces

Cédric Bellis, Bruno Lombard, Marie Touboul, Raphaël Assier

Effective dynamics for low-amplitude transient elastic waves in a 1D periodic array of non-linear interfaces

Cédric Bellis[1], Bruno Lombard[1], Marie Touboul[1], Raphaël Assier[2]

[1]Aix Marseille Univ, CNRS, Centrale Marseille, LMA, Marseille, France

[2]Department of Mathematics, The University of Manchester, Oxford Road, Manchester, M13 9PL, UK

Abstract

This article focuses on the time-domain propagation of elastic waves through a 1D periodic medium that contains non-linear imperfect interfaces, i.e. interfaces exhibiting a discontinuity in displacement and stress governed by a non-linear constitutive relation. The array considered is generated by a, possibly heterogeneous, cell repeated periodically and bonded by interfaces that are associated with transmission conditions of non-linear "spring-mass" type. More precisely, the imperfect interfaces are characterized by a linear dynamics but a non-linear elasticity law. The latter is not specified at first and only key theoretical assumptions are required. In this context, we investigate transient waves with both low-amplitude and long-wavelength, and aim at deriving homogenized models that describe their effective motion. To do so, the two-scale asymptotic homogenization method is deployed, up to the first-order. To begin, an effective model is obtained for the leading zeroth-order contribution to the microstructured wavefield. It amounts to a wave equation with a non-linear constitutive stress-strain relation that is inherited from the behavior of the imperfect interfaces at the microscale. The next first-order corrector term is then shown to be expressed in terms of a cell function and the solution of a linear elastic wave equation. Without further hypothesis, the constitutive relation and the source term of the latter depend non-linearly on the zeroth-order field, as does the cell function. Combining these zeroth- and first-order models leads to an approximation of both the macroscopic behavior of the microstructured wavefield and its small-scale fluctuations within the periodic array. Finally, particularizing for a prototypical non-linear interface law and in the cases of a homogeneous periodic cell and a bilaminated one, the behavior of the obtained models are then illustrated on a set of numerical examples and compared with full-field simulations. Both the influence of the dominant wavelength and of the wavefield amplitude are investigated numerically, as well as the characteristic features related to non-linear phenomena.

Keywords: Homogenization – Correctors – Imperfect interfaces – Non-linear waves – Time-domain numerical simulations

1 Introduction

This study concerns the propagation of elastic waves in structured media. When the waves are associated with wavelengths much larger than the characteristic length-scale of the propagating medium then some effective models can be derived to advantageously circumvent the complete description and computation of the fields at the microscopic scale. In such low-frequency and low-wavenumber settings, the field of dynamic homogenization has reached maturity and the macroscopic description of waves in periodic or random microstructures characterized by linear constitutive relations has been extensively studied, with techniques ranging from the two-scale homogenization method [8, 39], which we consider here, the Willis approach [45, 44, 34], or numerical multiscale methods, see e.g. the review in [1].

In the present work, we focus more specifically on periodic media that are structured by imperfect interfaces, which are associated with discontinuities of the displacement and stress fields along some internal contact areas, bonds or cracks. There exists a variety of models for such interfaces, which have been designed for applications to, e.g., composite materials, geophysics or non-destructive testing, see [42] for a comparative study. On the one hand, in the linear case, imperfect interface models amounts to typical "spring-mass" transmissions conditions, see [41, 6, 4, 38]. Note that some of these phenomenological models can also be seen as effective models for thin interphase bonds between solids, which has been demonstrated by asymptotic analysis [28, 26]. On the other hand, the use of non-linear transmission conditions can be necessary to model more complex interface phenomena, such as the generation of higher- or sub-harmonics, DC response, hysteretic or chaotic behaviors, slow dynamics, see e.g. [35, 9, 14]. In addition, non-linear parameters are generally more sensitive to the health state of materials than linear ones, which makes the modeling and measurements of non-linear phenomena appealing for non-destructive evaluation [43]. A widely considered non-linear model is the *non-smooth* unilateral contact model [37, 17]. For the present study, we rather focus on *smooth* non-linear interface laws, such as those that model elastic interphases or joints, see [2, 7]. Such compliant constitutive laws generally lead to problems that are mathematically well posed and that, as thus, can be properly handled numerically [31].

In the static regime the homogenization of heterogeneous media containing imperfect interfaces has been the subject of a number of studies, see e.g. [15, 16, 32]. In the dynamic regime however, the literature focusing on their effective behaviors is scarce, see [36, 33] and [3]. The latter study investigates theoretically the macroscopic motion of waves in a 1D periodic array of coated inclusions and matrix, with both the constituents and the interfaces behaving non-linearly. Here, we rather consider a 1D periodic array composed of a linear, and possibly heterogeneous material, bonded by imperfect interfaces that are governed by a smooth non-linear law. In this context, our primary objective is to describe the associated effective wave motion, both at the macroscopic and microscopic scales, in the long-wavelength regime and for low-amplitude forcings. At high-frequency, but only in the case of linear interfaces, the reader is kindly referred to our complementary study [5]. Our secondary objective is to analyze the mathematical properties of the homogenized models obtained and to assess them based on time-domain numerical simulations and comparisons with full-field simulations.

This article is organized as follows. The governing equations for the microstructured medium are introduced in Section 2 and our main homogenization results are stated. We proceed with some theoretical requirements on the constitutive parameters and functions, and provide an energy analysis of the microstructured wavefield. Considering both the macro- and micro-scale fluctuations of the latter relatively to a single parameter, namely the ratio of the period of the array to a characteristic wavelength, and low-amplitude excitations, then the two-scale homogenization method is deployed, while the non-linear interface law is kept generic during this analysis. The leading zeroth-order contributions to the microstructured wavefield are first derived in Section 3 and some properties of the effective model obtained are studied in Section 3.3. To approximate not only the macroscopic wave motion but also local fluctuations at the scale of the microstructure, first-order corrector terms are considered and studied in Section 4. To illustrate and assess the obtained effective models, at the zeroth- and first-order, Section 5 proposes a set of numerical experiments, with comparisons between full-field simulations in microstructured media and simulations involving their homogenized counterparts.

2 Wave propagation in a periodic array of interfaces

2.1 Research objectives

2.1.1 Formulation of the microstructured problem

We consider the propagation of transient waves in a 1D periodic elastic medium containing imperfect interfaces. The latter have spacing h and, for simplicity but with no loss of generality, we consider that they are located at $X_n = nh$ with $n \in \mathbb{Z}$. The elastic medium is supposed to be h-periodic and linear elastic with mass density $\rho_h(X)$ and Young's modulus $E_h(X)$. Given a source term F, the displacement field U_h is governed by the time-domain wave equation

$$\rho_h(X)\frac{\partial^2 U_h}{\partial t^2}(X,t) = \frac{\partial \Sigma_h}{\partial X}(X,t) + F(X,t) \qquad \text{where} \qquad \Sigma_h(X,t) = E_h(X)\frac{\partial U_h}{\partial X}(X,t), \tag{1}$$

with Σ_h being the stress field. Moreover, the interfaces are assumed to be characterized by the interface *mass* and *rigidity* parameters M and K, respectively, together with the, possibly *non-linear*, constitutive relation $\mathcal{R}$, so that the following transmission conditions apply at any interface point X_n, see [2, 7, 42, 9]:

$$\begin{cases} M\left\langle\!\!\left\langle \dfrac{\partial^2 U_h}{\partial t^2}(\cdot,t)\right\rangle\!\!\right\rangle_{X_n} = [\![\Sigma_h(\cdot,t)]\!]_{X_n} & \text{(2a)} \\ \langle\!\langle \Sigma_h(\cdot,t)\rangle\!\rangle_{X_n} = K\,\mathcal{R}\left([\![U_h(\cdot,t)]\!]_{X_n}\right), & \text{(2b)} \end{cases}$$

where, for any function $g(X)$, we define the jump and mean operators $[\![\cdot]\!]_{X_n}$ and $\langle\!\langle\cdot\rangle\!\rangle_{X_n}$ as

$$[\![g]\!]_{X_n} = g(X_n^+) - g(X_n^-) \qquad \text{and} \qquad \langle\!\langle g\rangle\!\rangle_{X_n} = \frac{1}{2}(g(X_n^+) + g(X_n^-)). \tag{3}$$

In addition, both the displacement U_h and the stress field Σ_h are continuous on the open intervals (X_n, X_{n+1}).

2.1.2 Main homogenization results

We now consider a reference wavelength λ^* and introduce the following parameters

$$k^* = \frac{2\pi}{\lambda^*} \qquad \text{and} \qquad \eta = hk^*, \tag{4}$$

k^* being the reference wavenumber. In this study it is assumed that $\eta \ll 1$ and that the source term F is of relatively *low-amplitude* (an issue that will be returned to hereinafter). The objective is to derive an effective dynamical model, up to the first-order, for the waves propagating in the periodic interface array considered. More precisely, we seek an approximation $U^{(1)}$ of the solution U_h to (1–2) of the form:

$$U_h(X,t) = U^{(1)}(X,t) + o(h).$$

The main results of this study is that the sought-after approximation is given by

$$U^{(1)}(X,t) = U_0(X,t) + hU_1(X,t), \tag{5}$$

where the zeroth-order field U_0 in (5) is continuous and is solution of the problem

$$\rho_{\text{eff}}\frac{\partial^2 U_0}{\partial t^2}(X,t) = \frac{\partial \Sigma_0}{\partial X}(X,t) + F(X,t) \qquad \text{with} \qquad \Sigma_0(X,t) = \mathcal{G}_{\text{eff}}(\mathcal{E}_0(X,t)).$$

Here, $\mathcal{E}_0 = \partial U_0/\partial X$ and $\mathcal{G}_{\text{eff}}$ is an effective strain-stress relation that is local and, generally speaking, non-linear, while ρ_{eff} is an effective mass density. This homogenized model is derived and detailed in Section 3. Moreover, the first-order corrector field U_1 in (5) can be written as

$$U_1(X,t) = \overline{U}_1(X,t) + \mathcal{P}\big(y, \mathcal{E}_0(X,t)\big)\, \mathcal{E}_0(X,t)$$

with $y = (X - nh)/h$ for $X \in (nh, (n+1)h)$ and where the *cell function* $\mathcal{P}$ is, generally speaking, a non-linear function of $\mathcal{E}_0$. The *mean* field $\overline{U}_1$ is solution to the *linear* problem:

$$\rho_{\text{eff}} \frac{\partial^2 \overline{U}_1}{\partial t^2}(X,t) = \frac{\partial \overline{\Sigma}_1}{\partial X}(X,t) + \mathcal{S}\big(U_0(X,t)\big) \qquad \text{with} \qquad \overline{\Sigma}_1(X,t) = \mathcal{G}'_{\text{eff}}\big(\mathcal{E}_0(X,t)\big)\, \overline{\mathcal{E}}_1(X,t),$$

where $\overline{\mathcal{E}}_1 = \partial \overline{U}_1/\partial X$, while both the *parameter* $\mathcal{G}'_{\text{eff}}(\mathcal{E}_0(X,t))$, which is the derivative of $\mathcal{G}_{\text{eff}}$, and the source term $\mathcal{S}\big(U_0(X,t)\big)$ depend explicitly on the zeroth-order field, locally in space and time, and in a non-linear fashion. This first-order homogenized model is derived in Section 4.

2.2 Main hypotheses

The constitutive parameters and functions characterizing the microstructured medium considered are assumed to satisfy the following mathematical assumptions.

Assumptions 1. *The mass density is expressed as $\rho_h(X) = \rho(X/h)$ and the Young's modulus reads $E_h(X) = E(X/h)$ where*

$$\rho, E \in L^\infty_{per}(0,1) := \Big\{ g \in L^\infty(\mathbb{R}),\ g(y+1) = g(y),\ \textit{a.e. } y \in \mathbb{R} \Big\},$$
$$\textit{with} \quad \rho \geq \rho_{min} > 0, \quad E \geq E_{min} > 0.$$

Assumptions 2. *The imperfect interfaces are such that $M \geq 0$ and $K > 0$, while $\mathcal{R}$ is a* smooth *function satisfying*

$$\mathcal{R} : (-d, +\infty) \longrightarrow \mathbb{R} \quad \textit{such that} \quad \mathcal{R}(0) = 0, \quad \mathcal{R}' > 0 \quad \textit{and} \quad (\mathcal{R}'' < 0 \ \textit{or}\ \mathcal{R}'' = 0),$$

where $d \in \mathbb{R}_+ \cup \{+\infty\}$ is a maximum compressibility length *and $\mathcal{R}'$, $\mathcal{R}''$ are the first and second derivatives of $\mathcal{R}$, respectively.*

In this article, the problem (1–2) will be investigated for a generic constitutive relation $\mathcal{R}$ but the particular case below will be considered in Section 5 for illustrative purposes.

Non-linear elastic interface model. A variety of non-linear interface models can be formulated within the framework of Assumptions 2. Without seeking to be exhaustive, we will be considering in Section 5 a non-linear model that is simple, but whose behavior is rich enough for illustrative purposes. The chosen model is a *hyperbolic* one, see [2, 7], with the function $\mathcal{R}$ being defined as

$$\mathcal{R}(\zeta) = \frac{\zeta}{1 + \zeta/d}, \tag{6}$$

where the compressibility length is finite with $d > 0$, see Figure 1. When this parameter degenerates as $d \to +\infty$, or when $\zeta \to 0$, then the non-linear model considered degenerates to a simple spring-like linear behavior for which the function $\mathcal{R}$ writes as

$$\mathcal{R}(\zeta) = \zeta. \tag{7}$$

Figure 2 illustrates the wave phenomena associated with the prototypical non-linear constitutive relation (6), by comparing snapshots of the (normalized) velocity field, defined as $V_h = \partial U_h/\partial t$

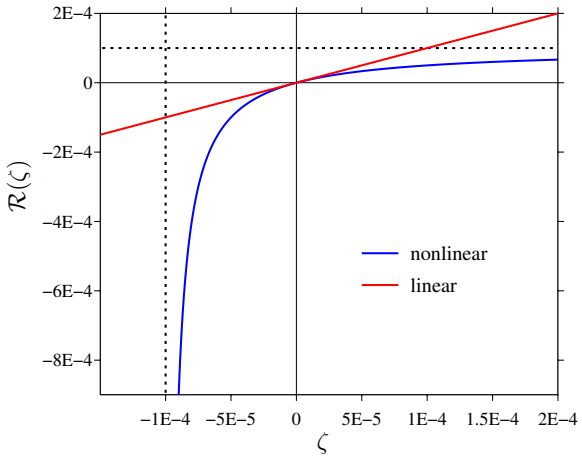

Figure 1: Hyperbolic interface law (6) and linear approximation. The dotted lines are placed at $\zeta = -d$ and $\mathcal{R} = d$.

and simulated within a microstructured medium with a homogeneous periodic cell. These are full-field simulations performed using the numerical methods described in Section 5. The amplitude of the generated waves is controlled by an amplitude parameter A in the source term F of (1). The interface are either linear or non-linear, i.e. characterized by (7) or (6), respectively. Figure 2 highlights that, at a small amplitude, the waveform within the non-linear microstructured medium is almost undistinguishable from that propagating within the linear one. Differences manifest themselves at larger amplitudes that sharpen the wave-fronts and increase high-frequency oscillations (which are associated with a dispersive, i.e. frequency-dependent, behavior). In other words increasing the forcing amplitude induces larger strains and thus stronger non-linear phenomena. Note that the wavefield is asymmetrical, unlike in the linear case, a phenomenon related to the asymmetry of the non-linear constitutive relation $\mathcal{R}$ in (6) that, because of a vertical asymptote at $-d$, is much stiffer in compression than in traction.

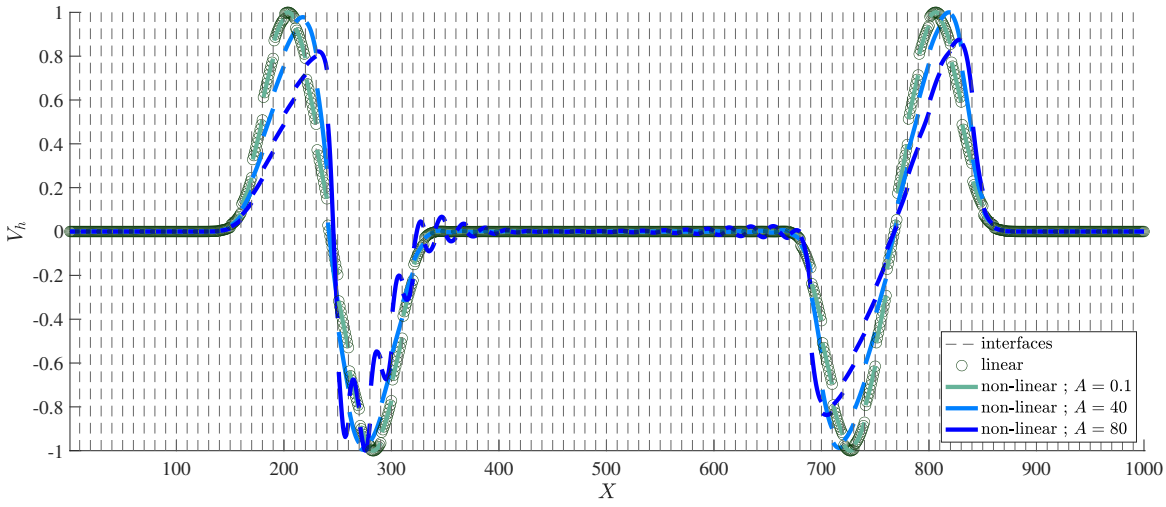

Figure 2: Snapshots of the wavefields V_h normalized at $t = 0.16\,\mathrm{s}$. These are simulated within a microstructured medium with a homogeneous periodic cell with $h = 10$ and containing either linear or non-linear interfaces (represented by vertical dashed lines). The corresponding physical parameters are provided in Section 5.3. The medium is excited by a source of central frequency $f_c = 10\,\mathrm{Hz}$ and a varying amplitude A.

These simulations highlight that, for a relatively low source amplitude, the wavefield exhibits small-scale fluctuations within the microstructure that are superposed to a large-scale non-linear macroscopic behavior. Capturing these features within effective models is the objective of the present study.

2.3 Energy analysis of the microstructured problem

Under the assumptions 1 and 2 considered, the existence and uniqueness of a solution to (1–2) has been proven in [18] in the case of a single interface and for a time-harmonic forcing. Here, we perform an energy analysis to show that these assumptions on the model parameters and constitutive function are also sufficient for the solution to be stable in the case of an array of interfaces. We consider the following definition.

Definition 1. *Consider an interval $I = [a, b]$ such that there does not exist $n \in \mathbb{Z}$ such that $a = nh$ or $b = nh$. We denote as $\{X_n^I\}$ the set of interface points X_n that are contained in I. Then, for all time $t \geq 0$, we define*

$$\begin{cases} \mathscr{E}_h^m(t) = \dfrac{1}{2}\displaystyle\int_I \left\{ \rho_h(X) V_h(X,t)^2 + \frac{1}{E_h(X)} \Sigma_h(X,t)^2 \right\} \mathrm{d}X, & \text{(8a)} \\ \mathscr{E}_h^i(t) = \displaystyle\sum_{X_n^I} \left\{ \frac{1}{2} M \langle\!\langle V_h(\cdot,t) \rangle\!\rangle_{X_n^I}^2 + K \int_0^{\mathcal{R}^{-1}\left(\langle\!\langle \Sigma_h(\cdot,t) \rangle\!\rangle_{X_n^I}/K\right)} \mathcal{R}(\zeta)\, \mathrm{d}\zeta \right\}, & \text{(8b)} \end{cases}$$

and $\mathscr{E}_h = \mathscr{E}_h^m + \mathscr{E}_h^i$.

With this definition at hand, then we can establish the following property, whose proof is deferred to Appendix A.

Property 1. *Owing to the assumptions 1 and 2 then $\mathscr{E}_h^m$ and $\mathscr{E}_h^i$ define respectively a* medium *mechanical energy and an* interface *energy for the system considered, with $\mathscr{E}_h^m(t) \geq 0$ and $\mathscr{E}_h^i(t) \geq 0$ for all $t \geq 0$. Moreover, $\mathscr{E}_h = 0$ if and only if $V_h = 0$ and $\Sigma_h = 0$ in I.*

Lastly, if V_h and Σ_h are compactly supported at time $t = 0$ then in the absence of source term, i.e. $F = 0$, it holds $\frac{\mathrm{d}}{\mathrm{d}t}\mathscr{E}_h = 0$ for all time t such that $\mathrm{supp}(V_h(\cdot,t)) \subset I$ and $\mathrm{supp}(\Sigma_h(\cdot,t)) \subset I$.

3 Zeroth-order homogenization

3.1 Two-scale expansion

We consider some reference material parameters ρ^* and E^* that define the wavespeed $c^* = \sqrt{E^*/\rho^*}$. These parameters will be specified later on. Accordingly and using (4), we introduce the following non-dimensionalized space and time variables $x = k^* X$ and $\tau = k^* c^* t$, respectively. Upon introducing the non-dimensionalized fields

$$u_\eta(x,\tau) = k^* U_h(X,t), \qquad v_\eta(x,\tau) = \frac{1}{c^*} V_h(X,t) \qquad \text{and} \qquad \sigma_\eta(x,\tau) = \frac{1}{E^*} \Sigma_h(X,t),$$

we have

$$v_\eta(x,\tau) = \frac{\partial u_\eta}{\partial \tau}(x,\tau) \qquad \text{and} \qquad \sigma_\eta(x,\tau) = \frac{1}{E^*} E\left(\frac{x}{\eta}\right) \frac{\partial u_\eta}{\partial x}(x,\tau).$$

The wave equation (1) can be recast as

$$\alpha\left(\frac{x}{\eta}\right) \frac{\partial^2 u_\eta}{\partial \tau^2}(x,\tau) = \frac{\partial}{\partial x}\left(\beta\left(\frac{x}{\eta}\right) \frac{\partial u_\eta}{\partial x}(x,\tau)\right) + f(x,\tau), \tag{9}$$

where we have defined

$$\alpha = \frac{\rho}{\rho^*},\ \beta = \frac{E}{E^*} \text{ in } L^\infty_{\text{per}}(0,1) \qquad \text{and} \qquad f(x,\tau) = \frac{F(X,t)}{k^* E^*}. \tag{10}$$

Moreover, the interface conditions (2) are recast as

$$\begin{cases} m\,\eta \left\langle\!\!\left\langle \dfrac{\partial^2 u_\eta}{\partial \tau^2}(\cdot,\tau) \right\rangle\!\!\right\rangle_{x_n} = \left[\!\!\left[\beta \dfrac{\partial u_\eta}{\partial x}(\cdot,\tau) \right]\!\!\right]_{x_n} \\ \left\langle\!\!\left\langle \beta \dfrac{\partial u_\eta}{\partial x}(\cdot,\tau) \right\rangle\!\!\right\rangle_{x_n} = \dfrac{k}{h}\,\mathcal{R}\left(\dfrac{h}{\eta} \left[\!\left[u_\eta(\cdot,\tau) \right]\!\right]_{x_n} \right) \end{cases} \qquad \text{with} \qquad m = \frac{M}{h\rho^*},\ k = \frac{Kh}{E^*}, \tag{11}$$

where we have extended the jump and mean notations at $x_n = nhk^* = n\eta$. The equations (9) and (11) are the non-dimensional counterparts of (1) and (2), respectively. As such, they fully highlight the contributions of the parameter η. Therefore, unless particular assumptions are made explicitly, the contribution of the terms in these equations, in particular that of the parameters α, β, m and k, will be of order $\mathcal{O}(1)$ in the forthcoming asymptotic expansion.

As discussed in Section 2.1.2, we assume that $\eta \ll 1$. In this context, the material parameters α and β vary on a fine scale associated with the rescaled coordinate $y = x/\eta$, see Figure 3. The wavefield is also assumed to have small-scale features that are described by y, and slow continuous variations as well, which can be described by the variable x, see Figure 2. Accordingly, the field u_η is expanded using the following ansatz:

$$u_\eta(x,\tau) = u_0(x,\tau) + \sum_{j\geq 1} \eta^j u_j(x, x/\eta, \tau), \tag{12}$$

where $u_0(x,\tau)$ embeds *large-scale* macroscopic variations while the fields $u_j(x,y,\tau)$ are associated with *micro-scale* localized fluctuations.

Remark 1. *In the case of linear interfaces, the fact that the leading-order term u_0 does not depend on the variable y can be proven rigorously. This result is here considered as a starting assumption for the asymptotic analysis.*

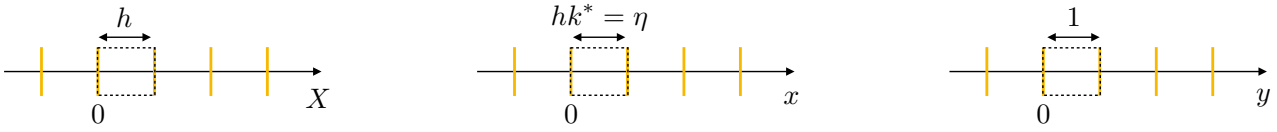

Figure 3: The different coordinates considered: *(left)* original coordinate, *(center)* adimensionalized coordinate, and *(right)* rescaled coordinate. The dashed boxes delimitate the chosen periodic cells.

The field u_0 is assumed to be continuous spatially and, for all $j \geq 1$, the fields u_j are assumed to be continuous with respect to the first variable and 1-periodic with respect to the second variable, i.e. $u_j(x,y,\tau) = u_j(x,y+1,\tau)$ for all $y \in (0,1)$, upon choosing the periodic cell as in Figure 3 with endpoints at $y_n = n$, with the following limit conditions:

$$u_j(x, y_n^+, \tau) = u_j(x, y_{n+1}^+, \tau) \qquad \text{and} \qquad u_j(x, y_n^-, \tau) = u_j(x, y_{n+1}^-, \tau). \tag{13}$$

The assumptions above will be tested and validated numerically in Section 5. Note that the periodic cell could have been defined as any translation of the one in Fig. 3, but the choice made here reduces

the number of unknowns in the forthcoming asymptotic analysis. The fields u_j being potentially discontinuous at the points y_n, we extend at the micro-scale the jump and mean notations (3) as

$$\begin{aligned}\llbracket u_j \rrbracket_{y_n} &\equiv \llbracket u_j(x,\cdot,\tau) \rrbracket_{y_n} = u_j(x,y_n^+,\tau) - u_j(x,y_{n+1}^-,\tau),\\ \langle\!\langle u_j \rangle\!\rangle_{y_n} &\equiv \langle\!\langle u_j(x,\cdot,\tau) \rangle\!\rangle_{y_n} = \frac{1}{2}(u_j(x,y_n^+,\tau) + u_j(x,y_{n+1}^-,\tau)).\end{aligned} \tag{14}$$

Remark 2. *Thereafter, the index will be dropped when the jump and mean refer specifically to the point $y_n = 0$, i.e. $\llbracket\cdot\rrbracket \equiv \llbracket\cdot\rrbracket_0$ and $\langle\!\langle\cdot\rangle\!\rangle \equiv \langle\!\langle\cdot\rangle\!\rangle_0$.*

As customary in this two-scale analysis, partial differentiation with respect to x has to be rewritten as $(\partial/\partial x + \frac{1}{\eta}\partial/\partial y)$ so that the non-dimentionalized wave equation (9) is recast as

$$\alpha(y)\frac{\partial^2 u_\eta}{\partial \tau^2} = \frac{1}{\eta^2}\frac{\partial}{\partial y}\left(\beta(y)\frac{\partial u_\eta}{\partial y}\right) + \frac{1}{\eta}\left(\frac{\partial}{\partial y}\left(\beta(y)\frac{\partial u_\eta}{\partial x}\right) + \beta(y)\frac{\partial^2 u_\eta}{\partial x \partial y}\right) + \beta(y)\frac{\partial^2 u_\eta}{\partial x^2} + f(x,\tau), \tag{15}$$

and the associated interface conditions (11) are

$$\begin{cases} m\,\eta\left\langle\!\!\left\langle \dfrac{\partial^2 u_\eta}{\partial \tau^2}\right\rangle\!\!\right\rangle_{y_n} = \left\llbracket \beta\left(\dfrac{\partial u_\eta}{\partial x} + \dfrac{1}{\eta}\dfrac{\partial u_\eta}{\partial y}\right)\right\rrbracket_{y_n} & \text{(16a)}\\ \left\langle\!\!\left\langle \beta\left(\dfrac{\partial u_\eta}{\partial x} + \dfrac{1}{\eta}\dfrac{\partial u_\eta}{\partial y}\right)\right\rangle\!\!\right\rangle_{y_n} = \dfrac{k}{h}\,\mathcal{R}\left(\dfrac{h}{\eta}\llbracket u_\eta \rrbracket_{y_n}\right), & \text{(16b)}\end{cases}$$

where the definitions (14) are being considered. Moreover, the continuity of the stress field within the periodic cells implies that $\beta\left(\frac{\partial u_\eta}{\partial x} + \frac{1}{\eta}\frac{\partial u_\eta}{\partial y}\right)$ is continuous on every intervals (y_n, y_{n+1}) and so is the term $\beta\left(\frac{\partial u_j}{\partial y} + \frac{\partial u_{j-1}}{\partial x}\right)$ for all $j \geq 1$.

Lastly, the source term F (resp. f) is also assumed to be of sufficiently low amplitude, a statement that will be returned to later on, so that the field U_h (resp. u_η) exhibits only moderate small-scale fluctuations within the microstructure, at least at sufficiently short times. In this context, the equations (15) and (16) will be used in the next section based on the ansatz (12).

3.2 Effective dynamical model

3.2.1 Model derivation

Consider the ansatz (12) in (16b). By definition we have $\llbracket u_0 \rrbracket_{y_n} = 0$ so that, given that the constitutive relation $\mathcal{R}$ characterizing the interface is a smooth function, we get the following relation from a Taylor expansion

$$\mathcal{R}\left(\frac{h}{\eta}\llbracket u_\eta \rrbracket_{y_n}\right) = \sum_{\ell \geq 0}\frac{(h\eta)^\ell}{\ell!}\left(\sum_{j\geq 2}\eta^{j-2}\llbracket u_j(x,\cdot,\tau)\rrbracket_{y_n}\right)^\ell \mathcal{R}^{(\ell)}\left(h\llbracket u_1(x,\cdot,\tau)\rrbracket_{y_n}\right) \tag{17}$$

where $\mathcal{R}^{(\ell)}$ denotes the ℓ-th derivative of $\mathcal{R}$.

Remark 3. *The assumption that the source term f is of low amplitude allows us to consider in the ensuing developments that, at least at sufficiently short times, the factors of the different powers of η in the expansion (17) are all of order $\mathcal{O}(1)$, i.e. they do not scale with η.*

Zeroth-order field. Owing to the assumption that u_0 is a macroscopic field independent of the small-scale variable y then the identification of the terms at order $\mathcal{O}(\eta^{-2})$ in (15) and $\mathcal{O}(\eta^{-1})$ in (16a) and (16b) does not bring additional information to it.

First-order field. Next, identifying the terms of order $\mathcal{O}(\eta^{-1})$ in (15) together with these of order $\mathcal{O}(1)$ in (16a) and (16b), given (17) and Remark 3, leads to the following system for the first-order field u_1:

$$\begin{cases} \dfrac{\partial}{\partial y}\left(\beta(y)\left(\dfrac{\partial u_1}{\partial y}(x,y,\tau)+\dfrac{\partial u_0}{\partial x}(x,\tau)\right)\right)=0, & \text{(18a)}\\ \left[\!\!\left[\beta\left(\dfrac{\partial u_1}{\partial y}+\dfrac{\partial u_0}{\partial x}\right)(x,\cdot,\tau)\right]\!\!\right]_{y_n}=0, & \text{(18b)}\\ \left\langle\!\!\left\langle\beta\left(\dfrac{\partial u_1}{\partial y}+\dfrac{\partial u_0}{\partial x}\right)(x,\cdot,\tau)\right\rangle\!\!\right\rangle_{y_n}=\dfrac{\not{k}}{h}\mathcal{R}\left(h\left[\!\!\left[u_1(x,\cdot,\tau)\right]\!\!\right]_{y_n}\right). & \text{(18c)}\end{cases}$$

Integration of (18a) with the continuity condition (18b) entails

$$\frac{\partial u_1}{\partial y}(x,y,\tau)=-\frac{\partial u_0}{\partial x}(x,\tau)+\frac{1}{\beta(y)}\sigma_0(x,\tau) \tag{19}$$

where σ_0 has to be determined. Considering averaging on the unit periodic cell as

$$\langle g\rangle=\int_0^1 g(y)\,\mathrm{d}y,$$

then for any continuous 1-periodic function on the open interval $(0,1)$ with limit conditions as in (13), i.e. with a potential discontinuity only at $y_n=0$, we have

$$\left\langle\frac{\mathrm{d}g}{\mathrm{d}y}\right\rangle=-\left[\!\!\left[g\right]\!\!\right]. \tag{20}$$

Applying this relation to u_1 leads to

$$\left\langle\frac{\partial u_1}{\partial y}(x,\cdot,\tau)\right\rangle=-\left[\!\!\left[u_1(x,\cdot,\tau)\right]\!\!\right] \tag{21}$$

Moreover, using (19) in (18c) and inverting the resulting equation leads to

$$\left[\!\!\left[u_1(x,\cdot,\tau)\right]\!\!\right]=\frac{1}{h}\mathcal{R}^{-1}\left(\frac{h}{\not{k}}\sigma_0(x,\tau)\right). \tag{22}$$

Averaging the equation (19), we may recall the definition (10) of β in terms of the reference modulus E^*. Setting the latter as follows

$$E^*=\left\langle\frac{1}{E}\right\rangle^{-1}\qquad\text{so that}\qquad\left\langle\frac{1}{\beta}\right\rangle=1, \tag{23}$$

then combining the equation (19) averaged with (21) and (22) finally leads to the following implicit local equation for σ_0:

$$\sigma_0(x,\tau)+\frac{1}{h}\mathcal{R}^{-1}\left(\frac{h}{\not{k}}\sigma_0(x,\tau)\right)=\varepsilon_0(x,\tau),$$

where $\varepsilon_0=\partial u_0/\partial x$. Formally, we introduce the inverse operator g_{eff} as

$$\sigma_0(x,\tau)=g_{\text{eff}}(\varepsilon_0(x,\tau)), \tag{24}$$

which constitutes the effective strain-stress relation to be used later on.

Second-order field. Considering the second-order field u_2, then identifying the terms of order $\mathcal{O}(1)$ in (15) gives

$$\frac{\partial}{\partial y}\left(\beta(y)\left(\frac{\partial u_2}{\partial y}(x,y,\tau)+\frac{\partial u_1}{\partial x}(x,y,\tau)\right)\right)+\beta(y)\frac{\partial^2 u_1}{\partial x\partial y}(x,y,\tau)+\beta(y)\frac{\partial^2 u_0}{\partial x^2}(x,\tau) \\ +f(x,\tau)=\alpha(y)\frac{\partial^2 u_0}{\partial \tau^2}(x,\tau), \quad (25)$$

and those of order $\mathcal{O}(\eta)$ in (16a) leads to

$$\left[\!\!\left[\beta\left(\frac{\partial u_2}{\partial y}+\frac{\partial u_1}{\partial x}\right)(x,\cdot,\tau)\right]\!\!\right]_{y_n}=m\left\langle\!\!\left\langle\frac{\partial^2 u_0}{\partial \tau^2}(x,\tau)\right\rangle\!\!\right\rangle_{y_n}. \quad (26)$$

Note that, for the purpose of deriving an effective model at the zeroth-order, there is no need to consider the $\mathcal{O}(\eta)$ contribution in equation (16b).

Averaging the equation (25) on the unit periodic cell $(0,1)$ while using the identity (20), given that $\beta\left(\frac{\partial u_2}{\partial y}+\frac{\partial u_1}{\partial x}\right)$ is continuous on $(0,1)$, together with the jump condition (26) implies

$$-m\left\langle\!\!\left\langle\frac{\partial^2 u_0}{\partial \tau^2}(x,\tau)\right\rangle\!\!\right\rangle+\frac{\partial}{\partial x}\left\langle\beta\left(\frac{\partial u_1}{\partial y}(x,\cdot,\tau)+\frac{\partial u_0}{\partial x}(x,\tau)\right)\right\rangle+f(x,\tau)=\langle\alpha\rangle\frac{\partial^2 u_0}{\partial \tau^2}(x,\tau). \quad (27)$$

Moreover, as in (23), the reference mass density entering the definition (10) of α is chosen as

$$\rho^*=\langle\rho\rangle \qquad \text{so that} \qquad \langle\alpha\rangle=1. \quad (28)$$

Finally, owing to the continuity of the field u_0 and using (19) in (27) we arrive at

$$(m+1)\frac{\partial^2 u_0}{\partial \tau^2}(x,\tau)=\frac{\partial}{\partial x}(\sigma_0(x,\tau))+f(x,\tau). \quad (29)$$

This equation constitutes the sought effective wave equation for the non-dimensionalized macroscopic field u_0 in the rescaled coordinate system.

3.2.2 Final homogenized model

To conclude, the equation (29) is transposed in the original coordinate system. From the definition of the non-dimensionalized variables and fields introduced in Section 3.1 and owing to (23) and (28), we consider the mean field $U_0(X,t)=u_0(x,\tau)/k^*$ that is governed by the equation

$$\rho_{\text{eff}}\frac{\partial^2 U_0}{\partial t^2}(X,t)=\frac{\partial \Sigma_0}{\partial X}(X,t)+F(X,t), \quad (30)$$

with the effective mass density being defined as

$$\rho_{\text{eff}}=\left(\langle\rho\rangle+\frac{M}{h}\right) \quad (31)$$

and the macroscopic stress field $\Sigma_0(X,t)=E^*\sigma_0(x,\tau)$ satisfying the following local and non-linear strain-stress relation

$$\left\langle\frac{1}{E}\right\rangle\Sigma_0(X,t)+\frac{1}{h}\mathcal{R}^{-1}\left(\frac{1}{K}\Sigma_0(X,t)\right)=\mathcal{E}_0(X,t), \quad (32)$$

where $\mathcal{E}_0=\partial U_0/\partial X$. The latter macroscopic strain field is therefore related to the macroscopic stress field Σ_0 by the effective constitutive relation (32), which we formally write as $\Sigma_0=\mathcal{G}_{\text{eff}}(\mathcal{E}_0)$.

Remark 4. *In the case of the linear interface law* (7)*, the effective strain-stress relation is linear and writes as*

$$\mathcal{G}_{\text{eff}}(\mathcal{E}_0) = \mathcal{C}^{\ell}_{\text{eff}}\,\mathcal{E}_0 \qquad \textit{with} \qquad \mathcal{C}^{\ell}_{\text{eff}} = \left(\left\langle \frac{1}{E} \right\rangle + \frac{1}{Kh}\right)^{-1}. \tag{33}$$

In addition, the case of perfect interfaces can be recovered by setting $K \to +\infty$ *and* $M \to 0$*, which yields the well known result* $\rho_{\text{eff}} \sim \langle \rho \rangle$ *and* $\mathcal{C}^{\ell}_{\text{eff}} \sim \langle 1/E \rangle^{-1}$*.*

Remark 5. *The zeroth-order stress-strain relation* $\Sigma_0 = \mathcal{G}_{\text{eff}}(\mathcal{E}_0)$*, in* (32) *or* (33)*, is local in space and time and, as such, applies to the static case as well (its derivation in (18–24) only involves equations that are time-independent). In such a static configuration, it could also be directly obtained from (1–2) as an exact relation between a macroscopic stress and an equivalent applied macroscopic strain associated with the prescribed body-force* F*.*

3.3 Properties

Now that the zeroth-order effective model (30–32) has been obtained, we are interested in characterizing its main properties.

3.3.1 Hyperbolicity

The equations (30–32) can be recast as the following first-order system:

$$\begin{cases} \dfrac{\partial \mathcal{E}_0}{\partial t}(X,t) = \dfrac{\partial V_0}{\partial X}(X,t) \\ \dfrac{\partial V_0}{\partial t}(X,t) = \dfrac{1}{\rho_{\text{eff}}} \left\{ \dfrac{\partial \Sigma_0(\mathcal{E}_0(X,t))}{\partial X} + F(X,t) \right\} \end{cases} \tag{34}$$

where the dependence of Σ_0 upon $\mathcal{E}_0$ through (32) has been emphasized. The non-linear system (34) can finally be written in condensed form as

$$\frac{\partial}{\partial t}\Psi_0(X,t) + \frac{\partial}{\partial X}\Big(\mathbb{G}_{\text{eff}}(\Psi_0(X,t))\Big) = \mathbb{F}(X,t) \qquad \text{with} \qquad \Psi_0 = (\mathcal{E}_0, V_0)^{\top}, \tag{35}$$

and where $\mathbb{G}_{\text{eff}}$ is a function from $\mathbb{R}^2$ into itself, while $\mathbb{F} = (0, F/\rho_{\text{eff}})^{\top}$. We then arrive at the main property below.

Property 2. *The non-linear first-order system* (35) *for the* zeroth-order field $(\mathcal{E}_0, V_0)$ *is a strictly hyperbolic system whose characteristic speeds, which are the eigenvalues of the Jacobian matrix* $\mathbb{G}'_{\text{eff}}$*, may be strain-dependent and write as* $\nu_{\pm}(\mathcal{E}_0) = \pm\sqrt{\dfrac{1}{\rho_{\text{eff}}}\dfrac{\partial \Sigma_0}{\partial \mathcal{E}_0}}$*.*
Moreover, except in the case of linear interfaces, the system (35) *is* genuinely non-linear*.*

The genuine non-linearity of hyperbolic systems is a fundamental property. It implies in particular that there exists a solution to the Cauchy problem, see [12], and that the waves connecting piecewise constant states are either shocks or rarefaction waves, a property that is at the foundation of some efficient numerical methods, see [13].

Proof. To prove Property 2, we consider the Jacobian matrix $\mathbb{G}'_{\text{eff}}(\Psi_0(X,t))$ associated with (35), which writes as

$$\mathbb{G}'_{\text{eff}}(\Psi_0(X,t)) = -\begin{pmatrix} 0 & 1 \\ \frac{1}{\rho_{\text{eff}}}\frac{\partial \Sigma_0}{\partial \mathcal{E}_0} & 0 \end{pmatrix}, \tag{36}$$

and whose eigenvalues are $\nu_\pm(\mathcal{E}_0) = \pm\sqrt{\frac{1}{\rho_{\text{eff}}}\frac{\partial\Sigma_0}{\partial\mathcal{E}_0}}$. Consider the effective strain-stress relation $\mathcal{E}_0 = \mathcal{G}_{\text{eff}}^{-1}(\Sigma_0)$ in (32). Since $\mathcal{R}$ is both a concave and strictly increasing function then $\mathcal{R}^{-1}$ is convex. Moreover, $\mathcal{R}^{-1}$ is also strictly increasing so that $\mathcal{G}_{\text{eff}}^{-1}$ is both convex and strictly increasing. As a consequence, $\mathcal{G}_{\text{eff}}$ is a concave and strictly increasing function. From that latter property, we get

$$\frac{\partial\Sigma_0}{\partial\mathcal{E}_0} = \mathcal{G}'_{\text{eff}}(\mathcal{E}_0) > 0,$$

which implies that the Jacobian matrix $\mathbb{G}'_{\text{eff}}$ has two distinct real eigenvalues. Therefore, (35) is a strictly hyperbolic system and the eigenvalues $\nu_\pm(\mathcal{E}_0)$ defined previously are its characteristic speeds. The corresponding right eigenvectors and the gradient of the eigenvalues with respect to Ψ_0 write as

$$r_\pm(\mathcal{E}_0) = \begin{pmatrix} 1 \\ \mp\sqrt{\frac{1}{\rho_{\text{eff}}}\partial\Sigma_0/\partial\mathcal{E}_0} \end{pmatrix} \qquad \text{and} \qquad \nabla\nu_\pm(\mathcal{E}_0) = \begin{pmatrix} \nu'_\pm(\mathcal{E}_0) \\ 0 \end{pmatrix},$$

with

$$\nu'_\pm(\mathcal{E}_0) = \pm\frac{1}{2\sqrt{\rho_{\text{eff}}\partial\Sigma_0/\partial\mathcal{E}_0}}\mathcal{G}''_{\text{eff}}(\mathcal{E}_0) = \mp\frac{1}{2\sqrt{\rho_{\text{eff}}\partial\Sigma_0/\partial\mathcal{E}_0}}\frac{(\mathcal{G}_{\text{eff}}^{-1})''(\Sigma_0)}{\Big[(\mathcal{G}_{\text{eff}}^{-1})'(\Sigma_0)\Big]^3}.$$

Now, from the definition (32) of the constitutive relation $\mathcal{G}_{\text{eff}}$ we have

$$(\mathcal{G}_{\text{eff}}^{-1})''(\Sigma_0) = \frac{1}{K^2h}(\mathcal{R}^{-1})''\left(\frac{1}{K}\Sigma_0(X,t)\right) = -\frac{1}{K^2h}\frac{\mathcal{R}''\Big(\mathcal{R}^{-1}(\Sigma_0(X,t)/K)\Big)}{\Big[\mathcal{R}'\Big(\mathcal{R}^{-1}(\Sigma_0(X,t)/K)\Big)\Big]^3} \geq 0,$$

which, under Assumptions 2, vanishes if and only if $\mathcal{R}'' = 0$, a condition that characterizes the case of linear elastic interfaces. It follows that $\nabla\nu_\pm^\top \cdot r_\pm \neq 0$ for all Ψ_0, and thus (35) is a genuinely non-linear hyperbolic system, see [13]. □

Remark 6. *At small strains, the effective stress-strain relation can be expanded at the second order as:*

$$\Sigma_0 \underset{\mathcal{E}_0\to 0}{\sim} \mathcal{G}'_{\text{eff}}(0)\,\mathcal{E}_0\,(1-\gamma\,\mathcal{E}_0) + o(\mathcal{E}_0^2) \qquad \textit{with} \qquad \mathcal{G}'_{\text{eff}}(0) > 0 \textit{ and } \gamma \geq 0, \tag{37}$$

since $\mathcal{G}_{\text{eff}}(0) = 0$ and given that $\mathcal{G}_{\text{eff}}$ is a concave and strictly increasing function. It is then possible to make use of the approximation (37) (resp. a polynomial approximation of $\mathcal{R}$) rather than of the exact relation $\mathcal{G}_{\text{eff}}$ (resp. $\mathcal{R}$). Nevertheless, if we do so, then the corresponding system (35) would only be conditionnally *hyperbolic, a property that is questionable from a modeling standpoint and prevent its use in standard time-domain simulation platforms. For these reasons, we prefer to keep the original constitutive law $\mathcal{R}$ in our model derivations.*

Remark 7. *Note that, if the constitutive relation $\mathcal{R}$ is a second-order polynomial, then it can be checked that the associated effective stress-strain relation (32) reduces to the result of [3].*

3.3.2 Energy analysis

To derive an energy conservation principle for the obtained local equations (30–32), we introduce again the velocity field $V_0 = \partial U_0/\partial t$ and consider the following definition.

Definition 2. *Consider an interval $I \subset \mathbb{R}$ and, for all time $t \geq 0$, define*

$$\mathscr{E}_0(t) = \int_I \left\{\frac{1}{2}\rho_{\text{eff}}V_0^2 + \mathcal{J}_{\text{eff}}\right\}\mathrm{d}X \qquad \textit{with} \qquad \mathcal{J}_{\text{eff}}(\mathcal{E}_0) = \int_0^{\mathcal{E}_0}\mathcal{G}_{\text{eff}}(\tilde{\mathcal{E}}_0)\,\mathrm{d}\tilde{\mathcal{E}}_0.$$

We can then establish the following property, whose proof is deferred to Appendix B.

Property 3. *Owing to the assumptions 1 and 2, $\mathscr{E}_0$ defines an effective mechanical energy associated with the zeroth-order homogenized model, such that $\mathscr{E}_0(t) \geq 0$ for all time $t \geq 0$.*

Moreover, $\mathscr{E}_0 = 0$ if and only if $V_0 = 0$ and $\mathcal{E}_0 = 0$ in I. Lastly, if V_0 and $\mathcal{E}_0$ are both sufficiently smooth and compactly supported at time $t = 0$ then in the absence of source term, i.e. $F = 0$, it holds $\frac{\mathrm{d}}{\mathrm{d}t}\mathscr{E}_0 = 0$ for all time t such that $\mathrm{supp}(V_0(\cdot, t)) \subset I$ and $\mathrm{supp}(\mathcal{E}_0(\cdot, t)) \subset I$.

Lastly, the effective energy $\mathscr{E}_0$ can be decomposed as $\mathscr{E}_0 = \mathscr{E}_0^m + \mathscr{E}_0^i$ with

$$\begin{cases} \mathscr{E}_0^m(t) = \dfrac{1}{2}\displaystyle\int_I \left\{ \langle \rho \rangle V_0^2 + \left\langle \frac{1}{E} \right\rangle \Sigma_0^2 \right\} \mathrm{d}X, & \text{(38a)} \\ \mathscr{E}_0^i(t) = \dfrac{1}{h}\displaystyle\int_I \left\{ \frac{1}{2} M V_0^2 + K \int_0^{\mathcal{R}^{-1}(\Sigma_0/K)} \mathcal{R}(\zeta)\, \mathrm{d}\zeta \right\} \mathrm{d}X. & \text{(38b)} \end{cases}$$

These terms are respectively associated with the bulk and interface energies of the microstructured problem, and satisfy $\mathscr{E}_0^m(t) \geq 0$ and $\mathscr{E}_0^i(t) \geq 0$ for all time $t \geq 0$.

Remark 8. *The proof of Property 3 in Appendix B is only based on the local equations (30–32) that define the effective model and the quantities (38a) and (38b) appear naturally in such a proof. Alternatively, their explicit form may have been deduced from the mechanical and interface energies characterizing the microstructured problem, see Definition 1. More precisely, provided that an appropriate adimensionalization of the latter is performed then the ansatz (12) can be employed directly so that the leading contribution can in turn be identified as the homogenized, zeroth-order, energy. Note however, that deriving the local effective equations from such energy quantities requires the use of a stationary principle, see e.g. the methodology employed in [25, 26].*

As shown in Property 1, which is relative to the microstructured problem, the total energy $\mathscr{E}_h$ is conserved in the absence of external sources. Moreover, the analogy is clearly observed between the corresponding energy terms in (8) and their counterparts (38) in the zeroth-order homogenized model, see also Remark 8. However, a fundamental difference occurs between the microstructured and homogenized models, due to the non-linearity of the partial differential equation (35), which allows the formation of shocks in a finite time. Note however that, according to Property 3, the total effective energy $\mathscr{E}_0$ is conserved as long as shocks do not appear. To better explain this property, we can exploit the analogy with another model widely studied in the context of gas dynamics: the so-called *p-system*, which describes, e.g., isentropic flows, with $p = -\Sigma_0$ and $u = \mathcal{E}_0$ with the notations of [12, Chapter 7]. Since the constitutive law $\mathcal{G}_{\text{eff}}$ is a concave and increasing function, the equivalent p-system has a decreasing and convex state equation $p(u)$. In this context, numerous theoretical results prove that classical solutions breakdown in a finite time for smooth initial data with compact support, see e.g. [23, 24, 12].

Considering the small strains quadratic non-linear constitutive law (37), then P. Lax derived an estimated time $t^\star$ when shocks would appear, see [23, 24]. Given a Cauchy problem with sinusoidal strain of amplitude $\mathcal{E}_{\max}$ and angular frequency $\omega_c = 2\pi f_c$, we obtain

$$t^\star \approx \frac{1}{\mathcal{E}_{\max} \gamma\, \omega_c} + \frac{1}{2 f_c}, \tag{39}$$

with the additional term $1/(2f_c)$ being the time required for the source to generate a complete sinus arch. Logically, $t^\star$ is inversely proportional to both the non-linearity coefficient γ of (37) and to the amplitude $\mathcal{E}_{\max}$, as the larger these parameters are the stronger the non-linear effects are. Shocks occur beyond $t^\star$ and the total energy $\mathscr{E}_0$ then decreases, contrary to the case of the microstructured

medium, see Section 3.3.1. Consequently, (39) can be interpreted as an upper bound of the duration of validity of the derived effective models. This issue will be illustrated by the numerical results of Section 5.

4 First-order homogenization

While the effective model obtained in Section 3.2 only involves the zeroth-order mean field U_0, the purpose of this section is to derive an enriched effective model up to the first-order. The derivation of this model follows the lines of Section 3.2 at the next order.

4.1 Model derivation

Identifying the terms of order $\mathcal{O}(\eta)$ in (15) gives

$$\frac{\partial}{\partial y}\left(\beta(y)\left(\frac{\partial u_3}{\partial y}(x,y,\tau)+\frac{\partial u_2}{\partial x}(x,y,\tau)\right)\right)+\beta(y)\frac{\partial^2 u_2}{\partial x\partial y}(x,y,\tau)+\beta(y)\frac{\partial^2 u_1}{\partial x^2}(x,y,\tau) \\ =\alpha(y)\frac{\partial^2 u_1}{\partial \tau^2}(x,y,\tau), \quad (40)$$

and, at the order $\mathcal{O}(\eta^2)$, the equation (16a) leads to

$$\left[\!\!\left[\beta\left(\frac{\partial u_3}{\partial y}+\frac{\partial u_2}{\partial x}\right)(x,\cdot,\tau)\right]\!\!\right]_{y_n}=\mathscr{m}\left\langle\!\!\left\langle\frac{\partial^2 u_1}{\partial \tau^2}(x,\cdot,\tau)\right\rangle\!\!\right\rangle_{y_n}. \quad (41)$$

Moreover, given (17) and Remark 3, the $\mathcal{O}(\eta)$ contribution in equation (16b) is

$$\left\langle\!\!\left\langle\beta\left(\frac{\partial u_2}{\partial y}+\frac{\partial u_1}{\partial x}\right)(x,\cdot,\tau)\right\rangle\!\!\right\rangle_{y_n}=\mathscr{k}\left[\!\!\left[u_2(x,\cdot,\tau)\right]\!\!\right]_{y_n}\mathcal{R}'\left(h\left[\!\!\left[u_1(x,\cdot,\tau)\right]\!\!\right]_{y_n}\right) \quad (42)$$

Averaging the equation (40) on the chosen unit periodic cell $(0,1)$ leads to

$$-\mathscr{m}\left\langle\!\!\left\langle\frac{\partial^2 u_1}{\partial \tau^2}(x,\cdot,\tau)\right\rangle\!\!\right\rangle+\frac{\partial}{\partial x}\left\langle\beta\left(\frac{\partial u_2}{\partial y}(x,\cdot,\tau)+\frac{\partial u_1}{\partial x}(x,\cdot,\tau)\right)\right\rangle=\left\langle\alpha\frac{\partial^2 u_1}{\partial \tau^2}(x,\cdot,\tau)\right\rangle, \quad (43)$$

where we have made use of (20), given that $\beta\left(\frac{\partial u_3}{\partial y}+\frac{\partial u_2}{\partial x}\right)$ is continuous on $(0,1)$, and (41). The identity will be used to derive an equation for the mean field $\langle u_1\rangle$ but, first, it leads us to make use of an explicit expression for the field u_1. To find one, the equation (19) is integrated as

$$u_1(x,y,\tau)=-\frac{\partial u_0}{\partial x}(x,\tau)\,y+\sigma_0(x,\tau)b(y)+q_1(x,\tau) \quad (44)$$

where σ_0 is given by (24), q_1 is to be determined, and the function $b(y)$ is defined as

$$b(y)=\int_0^y\frac{1}{\beta(z)}\,\mathrm{d}z.$$

Averaging the identity (44) gives

$$\langle u_1(x,\cdot,\tau)\rangle=-\frac{1}{2}\frac{\partial u_0}{\partial x}(x,\tau)+\mathcal{B}\,\sigma_0(x,\tau)+q_1(x,\tau) \quad (45)$$

with

$$\mathcal{B}=\langle b\rangle=\int_0^1\int_0^y\frac{1}{\beta(z)}\,\mathrm{d}z\,\mathrm{d}y.$$

Now, considering the first term in (43) we have

$$\left\langle\!\!\left\langle \frac{\partial^2 u_1}{\partial \tau^2}(x,\cdot,\tau) \right\rangle\!\!\right\rangle = \frac{\partial^2}{\partial \tau^2}\langle\!\langle u_1(x,\cdot,\tau)\rangle\!\rangle,$$

where owing to (14), (44) and (23), we have

$$\begin{aligned}
\langle\!\langle u_1(x,\cdot,\tau)\rangle\!\rangle &= \frac{1}{2}(u_1(x,0^+,\tau)+u_1(x,1^-,\tau)),\\
&= -\frac{1}{2}\frac{\partial u_0}{\partial x}(x,\tau)+\frac{1}{2}\sigma_0(x,\tau)+q_1(x,\tau),\\
&= \langle u_1(x,\cdot,\tau)\rangle + \left(\frac{1}{2}-\mathcal{B}\right)\sigma_0(x,\tau),
\end{aligned} \tag{46}$$

with the identity (45) being used at the last line to replace the still undetermined function q_1.

Next, in order to deal with the second term in (43), integrate the equation (25) and use the identity (19) to obtain the following:

$$\beta(y)\left(\frac{\partial u_2}{\partial y}(x,y,\tau)+\frac{\partial u_1}{\partial x}(x,y,\tau)\right)+\left(\frac{\partial \sigma_0}{\partial x}(x,\tau)+f(x,\tau)\right)y = a(y)\frac{\partial^2 u_0}{\partial \tau^2}(x,\tau)+p_2(x,\tau), \tag{47}$$

where the function $p_2(x,\tau)$ is to be determined and $a(y)$ is defined as

$$a(y)=\int_0^y \alpha(z)\,\mathrm{d}z.$$

To determine the function p_2, divide (47) through by β, average the resulting equation on the unit cell $(0,1)$ and use the identities (20) and (23) to obtain

$$-[\![u_2(x,\cdot,\tau)]\!]+\frac{\partial}{\partial x}\langle u_1(x,\cdot,\tau)\rangle+\left(\frac{\partial \sigma_0}{\partial x}(x,\tau)+f(x,\tau)\right)\left\langle\frac{y}{\beta}\right\rangle = \frac{\partial^2 u_0}{\partial \tau^2}(x,\tau)\left\langle\frac{a}{\beta}\right\rangle+p_2(x,\tau). \tag{48}$$

Moreover, considering the left-hand side of equation (42), then from (14), (47) and (28) we get

$$\left\langle\!\!\left\langle \beta\left(\frac{\partial u_2}{\partial y}+\frac{\partial u_1}{\partial x}\right)(x,\cdot,\tau)\right\rangle\!\!\right\rangle = \frac{1}{2}\frac{\partial^2 u_0}{\partial \tau^2}(x,\tau)-\frac{1}{2}\left(\frac{\partial \sigma_0}{\partial x}(x,\tau)+f(x,\tau)\right)+p_2(x,\tau),$$

which, once replaced in (42), entails

$$[\![u_2(x,\cdot,\tau)]\!] = \frac{1}{\not{k}\mathcal{R}'\left(h\,[\![u_1(x,\cdot,\tau)]\!]\right)}\left\{\frac{1}{2}\frac{\partial^2 u_0}{\partial \tau^2}(x,\tau)-\frac{1}{2}\left(\frac{\partial \sigma_0}{\partial x}(x,\tau)+f(x,\tau)\right)+p_2(x,\tau)\right\}. \tag{49}$$

Making use of (49) in (48) leads to the following expression for the sought function p_2:

$$p_2(x,\tau) = c_{\mathrm{eff}}(\varepsilon_0)\left\{\frac{\partial}{\partial x}\langle u_1(x,\cdot,\tau)\rangle - d_0(\varepsilon_0)\frac{\partial^2 u_0}{\partial \tau^2}(x,\tau)+d_1(\varepsilon_0)\left(\frac{\partial \sigma_0}{\partial x}(x,\tau)+f(x,\tau)\right)\right\} \tag{50}$$

where we have introduced the quantities

$$\begin{cases}
c_{\mathrm{eff}}(\varepsilon_0(x,\tau)) = \left(1+\dfrac{1}{\not{k}\,\phi(\varepsilon_0(x,\tau))}\right)^{-1}\\[2ex]
d_0(\varepsilon_0(x,\tau)) = \left\langle\dfrac{a}{\beta}\right\rangle+\dfrac{1}{2\not{k}\,\phi(\varepsilon_0(x,\tau))} \qquad \text{with} \qquad \phi(\varepsilon_0(x,\tau)) = \mathcal{R}'\left(h\,[\![u_1(x,\cdot,\tau)]\!]\right),\\[2ex]
d_1(\varepsilon_0(x,\tau)) = \left\langle\dfrac{y}{\beta}\right\rangle+\dfrac{1}{2\not{k}\,\phi(\varepsilon_0(x,\tau))}
\end{cases}$$

which all depend on the zeroth-order strain field ε_0 through $[\![u_1(x,\cdot,\tau)]\!]$ owing to the identities (22) and (24). Note that these quantities may be employed while omitting the x and τ variables for conciseness. Moreover, using the link between g_{eff} and $\mathcal{R}$, and the formula for derivatives of inverse functions, it is straightforward to show the following property.

Property 4. *It holds* $c_{\text{eff}}(\varepsilon_0) = g'_{\text{eff}}(\varepsilon_0)$.

Back to the calculation of the second term in (43), the equation (47) is averaged on the unit cell $(0,1)$ and (50) is used to obtain

$$\left\langle \beta \left(\frac{\partial u_2}{\partial y}(x,\cdot,\tau) + \frac{\partial u_1}{\partial x}(x,\cdot,\tau) \right) \right\rangle = g'_{\text{eff}}(\varepsilon_0) \frac{\partial}{\partial x} \langle u_1(x,\cdot,\tau) \rangle + (\mathcal{A} - g'_{\text{eff}}(\varepsilon_0) d_0(\varepsilon_0)) \frac{\partial^2 u_0}{\partial \tau^2}(x,\tau) + \left(g'_{\text{eff}}(\varepsilon_0) d_1(\varepsilon_0) - \frac{1}{2} \right) \left(\frac{\partial \sigma_0}{\partial x}(x,\tau) + f(x,\tau) \right),$$

where we have defined

$$\mathcal{A} = \langle a \rangle = \int_0^1 \int_0^y \alpha(z) \, \mathrm{d}z \, \mathrm{d}y.$$

Finally, making use of the expression (24) for σ_0 and of the zeroth-order equation (29) yields

$$\left\langle \beta \left(\frac{\partial u_2}{\partial y}(x,\cdot,\tau) + \frac{\partial u_1}{\partial x}(x,\cdot,\tau) \right) \right\rangle = g'_{\text{eff}}(\varepsilon_0) \frac{\partial}{\partial x} \langle u_1(x,\cdot,\tau) \rangle + \left(\mathcal{A} - g'_{\text{eff}}(\varepsilon_0) d_0(\varepsilon_0) + \left(g'_{\text{eff}}(\varepsilon_0) d_1(\varepsilon_0) - \frac{1}{2} \right) (m+1) \right) \frac{\partial^2 u_0}{\partial \tau^2}(x,\tau). \quad (51)$$

In a last step we focus on the right-hand side term in (43). As the unit cell is not necessarily homogeneous in terms of mass density then that term is recast as follows

$$\left\langle \alpha \frac{\partial^2 u_1}{\partial \tau^2}(x,\cdot,\tau) \right\rangle = \frac{\partial^2}{\partial \tau^2} \langle \alpha \, u_1(x,\cdot,\tau) \rangle .$$

Moreover, we can make use of the identity (44) for u_1 together with (28) and (45) to obtain

$$\begin{aligned} \langle \alpha \, u_1(x,\cdot,\tau) \rangle &= -\frac{\partial u_0}{\partial x}(x,\tau) \langle \alpha \, y \rangle + \sigma_0(x,\tau) \langle \alpha \, b \rangle + q_1(x,\tau) \\ &= \langle u_1(x,\cdot,\tau) \rangle + \left(\frac{1}{2} - \langle \alpha \, y \rangle \right) \frac{\partial u_0}{\partial x}(x,\tau) + (\langle \alpha \, b \rangle - \mathcal{B}) \sigma_0(x,\tau) \end{aligned} \quad (52)$$

To conclude, the identities (46), (51) and (52) are used back in (43). Doing so we obtain the equation below for the mean field $\langle u_1 \rangle$:

$$(m+1) \frac{\partial^2}{\partial \tau^2} \langle u_1(x,\cdot,\tau) \rangle = \frac{\partial}{\partial x} (\overline{\sigma}_1(x,\tau)) + s(u_0(x,\tau)) \quad (53)$$

with $\overline{\sigma}_1$ being a macroscopic stress defined as

$$\overline{\sigma}_1(x,\tau) = g'_{\text{eff}}(\varepsilon_0(x,\tau)) \frac{\partial}{\partial x} \langle u_1(x,\cdot,\tau) \rangle ,$$

and where the source term $s(u_0(x,\tau))$ is given by

$$s(u_0(x,\tau)) = \frac{\partial}{\partial x} \left(g'_{\text{eff}}(\varepsilon_0) \Big\{ (m+1) d_1(\varepsilon_0) - d_0(\varepsilon_0) \Big\} \frac{\partial^2 u_0}{\partial \tau^2}(x,\tau) \right) + \left\{ \mathcal{A} + \langle \alpha \, y \rangle - \frac{m}{2} - 1 \right\} \frac{\partial^3 u_0}{\partial x \partial \tau^2}(x,\tau) + \left\{ \mathcal{B} - \langle \alpha \, b \rangle + m \left(\mathcal{B} - \frac{1}{2} \right) \right\} \frac{\partial^2 \sigma_0}{\partial \tau^2}(x,\tau). \quad (54)$$

In the present form, the source term (54) is not quite tractable. However, based on the calculations of Appendix C, it turns out to satisfy the following property.

Property 5. *For all x and τ, the source term (54) is identically equal to*

$$s(u_0) = \mathcal{C}\, g''_{\text{eff}}(\varepsilon_0) \left\{ \left(\frac{\partial^2 u_0}{\partial x \partial \tau} \right)^2 - \frac{\partial^2 u_0}{\partial x^2} \frac{\partial^2 u_0}{\partial \tau^2} \right\}$$

where $\mathcal{C} = \left\{ \mathcal{B} - \langle \alpha\, b \rangle + m \left(\mathcal{B} - \frac{1}{2} \right) \right\}$. *Moreover, when the periodic cell is homogeneous (without restriction on the linearity or non-linearity of the interface) we have* $\mathcal{C} = 0$, *while for linear interfaces we have* $g''_{\text{eff}} = 0$. *Hence,* $s(u_0) = 0$ *in both of these cases.*

Finally, once the mean field is computed using the equation (53), then the local *corrector* u_1 at the micro-scale within the periodic array can be reconstructed by combining the equations (44) and (45) as

$$u_1(x, y, \tau) = \langle u_1(x, \cdot, \tau) \rangle + \left(\frac{1}{2} - y \right) \varepsilon_0(x, \tau) + \left(b(y) - \mathcal{B} \right) g_{\text{eff}}(\varepsilon_0(x, \tau)). \tag{55}$$

4.2 First-order homogenized model

4.2.1 Final model

Now that the model has been obtained for the first-order term u_1 in the rescaled coordinate system, the final step is to formulate the sought first-order approximation of the solution U_h in the original coordinate system, as discussed in Section 2.1.2. Considering the ansatz (12), then from u_0 and u_1 we can define the approximation $u^{(1)}$ as

$$u^{(1)}(x, \tau) = u_0(x, \tau) + \eta u_1(x, x/\eta, \tau) = u_0(x, \tau) + h k^* u_1(x, x/\eta, \tau),$$

which, transposed in the original coordinate system, is expressed as

$$U^{(1)}(X, t) = U_0(X, t) + h U_1(X, t), \tag{56}$$

where $U^{(1)}(X, t) = u^{(1)}(x, \tau)/k^*$ and, by a slight abuse of notation, $U_1(X, t) = u_1(x, x/\eta, \tau)$. The equations satisfied by U_1 are now provided below.

Considering the mean displacement field $\overline{U}_1(X, t) = \langle u_1(x, \cdot, \tau) \rangle$, the latter is governed by the following equation

$$\rho_{\text{eff}} \frac{\partial^2 \overline{U}_1}{\partial t^2}(X, t) = \frac{\partial \overline{\Sigma}_1}{\partial X}(X, t) + \mathcal{S}(U_0(X, t)), \tag{57}$$

where (31) has been used. Here the macroscopic stress field $\overline{\Sigma}_1(X, t) = k^* E^* \overline{\sigma}_1(x, \tau)$ satisfies the following *linear* and *heterogeneous* constitutive relation

$$\overline{\Sigma}_1(X, t) = \mathcal{G}'_{\text{eff}}(\mathcal{E}_0(X, t)) \frac{\partial \overline{U}_1}{\partial X}(X, t), \tag{58}$$

while, according to Property 5, the source term $\mathcal{S}(U_0)$ is given by

$$\mathcal{S}(U_0(X, t)) = \langle \rho \rangle \left\langle \frac{1}{E} \right\rangle \left\{ \mathcal{B} - \langle \alpha\, b \rangle + \frac{M}{h \langle \rho \rangle} \left(\mathcal{B} - \frac{1}{2} \right) \right\} \mathcal{G}''_{\text{eff}}(\mathcal{E}_0) \left\{ \left(\frac{\partial^2 U_0}{\partial X \partial t} \right)^2 - \frac{\partial^2 U_0}{\partial X^2} \frac{\partial^2 U_0}{\partial t^2} \right\}.$$

Moreover, once the mean field $\overline{U}_1(X, t)$ has been computed then the associated local corrector, i.e. the *total field* $U_1(X, t) = u_1(x, y, \tau)$ can be found by expressing (55) in the original coordinate system with $y = (X - nh)/h$ when X belongs to a given interval $(nh, (n+1)h)$, so that

$$\begin{aligned} U_1(X, t) &= \overline{U}_1(X, t) + \mathcal{P}(y, \mathcal{E}_0(X, t))\, \mathcal{E}_0(X, t), \\ \text{with} \qquad \mathcal{P}(y, \mathcal{E}_0(X, t)) &= \left(\frac{1}{2} - y \right) + \left(b(y) - \mathcal{B} \right) \left\langle \frac{1}{E} \right\rangle \frac{\mathcal{G}_{\text{eff}}(\mathcal{E}_0(X, t))}{\mathcal{E}_0(X, t)}. \end{aligned} \tag{59}$$

Note that, in the above, $\mathcal{P}$ is a *cell function* that, generally speaking, depends explicitly and in a non-linear fashion on $\mathcal{E}_0(X,t)$. Given the definition (32) of $\mathcal{G}_{\text{eff}}$ that features the interface law $\mathcal{R}$ and owing to Assumptions 2, then we immediately arrive at the property below.

Property 6. *The parameter $\mathcal{G}'_{\text{eff}}(\mathcal{E}_0(X,t))$ entering the effective constitutive relation (58) satisfies $\mathcal{G}'_{\text{eff}}(\mathcal{E}_0(X,t)) > 0$ at all point X and time t so that the problem (57–58) is well posed.*

Remark 9. *In the case of linear interfaces, see (7) and Remark 4, then we get $\mathcal{G}'_{\text{eff}}(\mathcal{E}_0(X,t)) = \mathcal{C}^{\ell}_{\text{eff}}$ and $\mathcal{S}(U_0(X,t)) = 0$. In addition, since $\mathcal{G}_{\text{eff}}(\mathcal{E}_0)/\mathcal{E}_0 = \mathcal{C}^{\ell}_{\text{eff}}$ then the cell function $\mathcal{P}$ in (59) only depends on the coordinate y and reduces to a known form, see e.g. [10].*

4.2.2 Hyperbolic system

As previously done in Section 3.3.1 with the zeroth-order model, the equations (57–58) for the mean field $\overline{U}_1(X,t)$ can be recast as the following first-order system:

$$\begin{cases} \dfrac{\partial \overline{\mathcal{E}}_1}{\partial t}(X,t) = \dfrac{\partial \overline{V}_1}{\partial X}(X,t), \\ \dfrac{\partial \overline{V}_1}{\partial t}(X,t) = \dfrac{1}{\rho_{\text{eff}}} \left\{ \dfrac{\partial}{\partial X} \left(\mathcal{G}'_{\text{eff}}(\mathcal{E}_0(X,t)) \overline{\mathcal{E}}_1(X,t) \right) + \mathcal{S}(U_0(X,t)) \right\} \end{cases} \tag{60}$$

with $\overline{V}_1 = \partial \overline{U}_1/\partial t$ and $\overline{\mathcal{E}}_1 = \partial \overline{U}_1/\partial X$. In turn, and with the notation of (35), the linear system (60) can be written in condensed form as

$$\frac{\partial}{\partial t} \overline{\Psi}_1(X,t) + \frac{\partial}{\partial X} \left(\mathbb{G}'_{\text{eff}}(\Psi_0(X,t)) \, \overline{\Psi}_1(X,t) \right) = \mathbb{S}(\Psi_0(X,t)) \qquad \text{with} \qquad \overline{\Psi}_1 = (\overline{\mathcal{E}}_1, \overline{V}_1)^{\top}, \tag{61}$$

and where $\mathbb{G}'_{\text{eff}}(\Psi_0(X,t))$ is the Jacobian matrix (36) of the system (35) governing the zeroth-order field $\Psi_0 = (\mathcal{E}_0, V_0)^{\top}$, while $\mathbb{S} = (0, \mathcal{S}(U_0)/\rho_{\text{eff}})^{\top}$. As a consequence, the Jacobian matrix of the system (61) is also equal to the matrix $\mathbb{G}'_{\text{eff}}(\Psi_0(X,t))$, so that, owing to Property 2, we immediately arrive at the following result.

Property 7. *The first-order system (61) for the* first-order mean field $(\overline{\mathcal{E}}_1, \overline{V}_1)$ *is a linear and strictly hyperbolic system, whose characteristic speeds are identically equal to these of the first-order system (35), namely $\nu_{\pm}(\mathcal{E}_0)$, for the* zeroth-order field $(\mathcal{E}_0, V_0)$.

5 Numerical experiments

In this section, the zeroth- and first-order effective models derived previously for any constitutive relation $\mathcal{R}$ are illustrated using time-domain numerical simulations and considering the hyperbolic non-linear constitutive relation (6), which is both simple and rich enough to highlight typical non-linear phenomena. Moreover, in all of the numerical examples considered hereafter, we place ourselves in the particular case where $M = 0$ in (2a), so as to focus on the non-linear effects that stems only from the transmission condition (2b). Physically, this corresponds to configurations where the mass density of the elastic interphase or joint is much smaller than that of the bonded materials, so that it can thus be neglected.

5.1 Effective model

Starting with the zeroth-order homogenized model, then making use of (6) in (32) leads to a quadratic equation for Σ_0 whose solution satisfying $\Sigma_0 = 0$ when $\mathcal{E}_0 = 0$ writes as an effective constitutive relation

$\Sigma_0 = \mathcal{G}_{\text{eff}}(\mathcal{E}_0)$ of the form:

$$\Sigma_0 = \frac{1}{2\mathcal{C}^\ell_{\text{eff}}}\left\langle \frac{1}{E}\right\rangle^{-1}\left\{ Kd + \mathcal{C}^\ell_{\text{eff}}\,\mathcal{E}_0 - \left[\left(Kd + \mathcal{C}^\ell_{\text{eff}}\,\mathcal{E}_0\right)^2 - 4\left\langle \frac{1}{E}\right\rangle Kd(\mathcal{C}^\ell_{\text{eff}})^2\,\mathcal{E}_0\right]^{1/2}\right\}, \tag{62}$$

with $\mathcal{C}^\ell_{\text{eff}}$ being the effective stiffness (33) of the linear interface case, see Figure 4-(b). We can deduce the following limit behaviors:

$$\Sigma_0 \underset{\mathcal{E}_0\to-\infty}{\sim} \left\langle \frac{1}{E}\right\rangle^{-1}\mathcal{E}_0 \qquad \text{and} \qquad \lim_{\mathcal{E}_0\to+\infty}\Sigma_0 = Kd. \tag{63}$$

These limits can easily be interpreted from a phenomenological viewpoint. On the one hand, given that the hyperbolic law (6) has a vertical asymptote at $\zeta = -d$, see Figure 1, then the secant modulus of the interfaces, i.e. the ratio $\mathcal{R}(\zeta)/\zeta$, tends to infinity in compression. It then becomes very expensive energetically to deform them, so that the deformation of the microstructured medium concentrates in the elastic cells in compression. Therefore, it is only the elasticity of the latter that is seen macroscopically in the limit $\mathcal{E}_0 \to -\infty$. On the other hand, the law (6) has a horizontal asymptote at $\mathcal{R} = +d$ with the associated secant modulus tending to zero when $\mathcal{E}_0 \to +\infty$. As a consequence, when solicited in traction, the deformation localizes in the interfaces rather than in the elastic cells, as it is more advantageous energetically. Asymptotically, it is thus only the stiffness of the former that is seen macroscopically.

In the case of (62), the small strains second-order Taylor expansion (37) writes as

$$\Sigma_0 \underset{\mathcal{E}_0\to0}{\sim} \mathcal{C}^\ell_{\text{eff}}\,\mathcal{E}_0\,(1-\gamma\,\mathcal{E}_0) + o(\mathcal{E}_0^2) \qquad \text{with} \qquad \gamma = \frac{1}{hd}\left(\frac{\mathcal{C}^\ell_{\text{eff}}}{K}\right)^2 > 0. \tag{64}$$

As a consequence, at small strains, the effective behavior is linear, with modulus $\mathcal{C}^\ell_{\text{eff}}$, and non-linear effects are governed by the parameter γ and increase with the strain amplitude, comparatively.

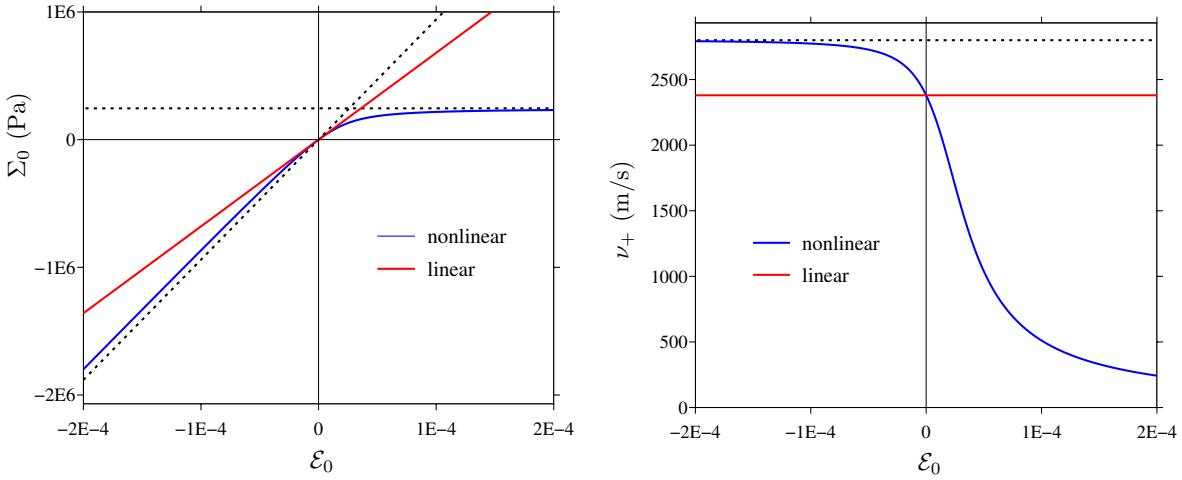

(a) Non-linear constitutive relation $\Sigma_0 = \mathcal{G}_{\text{eff}}(\mathcal{E}_0)$ in (62) and linear case $\Sigma_0 = \mathcal{C}^\ell_{\text{eff}}\,\mathcal{E}_0$ in (33).

(b) Sound speeds $\nu_+(\mathcal{E}_0)$ in (65) and ν^ℓ_+ for the linear case.

Figure 4: Properties of the zeroth-order homogenized model. The numerical values of the associated physical parameters are provided in Section 5.3. The dotted lines denote the theoretical asymptotic behaviors.

The characteristic speeds, see Property 2, associated with (62) depend explicitly on the strain $\mathcal{E}_0$

and write as:

$$\nu_\pm(\mathcal{E}_0)^2 = \frac{1}{2\rho_{\text{eff}}}\left\langle\frac{1}{E}\right\rangle^{-1}\left\{1 - \frac{Kd + \mathcal{C}^\ell_{\text{eff}}\,\mathcal{E}_0 - 2\,\langle 1/E\rangle\,Kd\,\mathcal{C}^\ell_{\text{eff}}}{\left[\left(Kd + \mathcal{C}^\ell_{\text{eff}}\,\mathcal{E}_0\right)^2 - 4\,\langle 1/E\rangle\,Kd\,(\mathcal{C}^\ell_{\text{eff}})^2\,\mathcal{E}_0\right]^{1/2}}\right\}. \tag{65}$$

Remark 10. *In the particular case of linear interfaces, i.e. when $\mathcal{R}(\zeta) = \zeta$, we recover the linear constitutive law $\Sigma_0 = \mathcal{C}^\ell_{\text{eff}}\,\mathcal{E}_0$ of Remark 4, whose associated characteristic speeds are $\nu^\ell_\pm = \pm\sqrt{\mathcal{C}^\ell_{\text{eff}}/\rho_{\text{eff}}}$.*

As theoretically analyzed, the $\nu_\pm$ in (65) are real-valued for all $\mathcal{E}_0$. Moreover, from (63–64), we get:

$$\lim_{\mathcal{E}_0\to-\infty}\nu_\pm(\mathcal{E}_0) = \pm\sqrt{\frac{1}{\rho_{\text{eff}}}\left\langle\frac{1}{E}\right\rangle^{-1}}, \qquad \nu_\pm(0) = \nu^\ell_\pm, \qquad \lim_{\mathcal{E}_0\to+\infty}\nu_\pm(\mathcal{E}_0) = 0.$$

The constitutive law (62) and the linear approximation (33) are illustrated on Figure 4a, using the physical parameters that characterize the homogeneous periodic cell described in Section 5.3. The associated wave speeds are illustrated on Figure 4b.

Regarding the first-order homogenized model, see (56) together with the first-order corrector (59), then we have $\mathcal{G}_{\text{eff}}(\mathcal{E}_0)/\mathcal{E}_0 \sim \mathcal{C}^\ell_{\text{eff}}$ both for the non-linear law (6) in the limit of small strains, see (64), and in the linear case (7). Hence, the cell function $\mathcal{P}$ in (59) does not depend on $\mathcal{E}_0$ in such cases. In the non-linear case and at larger strains then $\mathcal{E}_0$ acts as a parameter for $\mathcal{P}$. To illustrate this, and in accordance with the numerical results presented hereafter, we consider its companion *velocity-based* cell function $\mathcal{P}_V$, which is defined through the following identity:

$$\begin{aligned} V^{(1)}(X,t) = \frac{\partial U^{(1)}}{\partial t}(X,t) &= V_0(X,t) + h\overline{V}_1(X,t) + h\,\mathcal{P}_V(y,\mathcal{E}_0(X,t))\,\frac{\partial V_0}{\partial X}(X,t) \\ \text{with} \qquad \mathcal{P}_V(y,\mathcal{E}_0(X,t)) &= \left(\frac{1}{2} - y\right) + (b(y) - \mathcal{B})\left\langle\frac{1}{E}\right\rangle\mathcal{G}'_{\text{eff}}(\mathcal{E}_0(X,t)), \end{aligned} \tag{66}$$

and where $V_0 = \partial U_0/\partial t$ and $\overline{V}_1 = \partial\overline{U}_1/\partial t$. Then the behavior of $\mathcal{P}_V$ is illustrated on Figure 5 for two different material configurations, namely a homogeneous periodic cell and a bilaminated one.

Lastly, and to follow up on Section 3.3.1, we can particularize the estimated time $t^\star$ in (39). In the linear case, i.e. in the small strain limit, a monochromatic forcing of amplitude A leads to $\mathcal{E}_{\max} = A/(\nu^\ell_+)^2$. Given the coefficient γ in (64), this yields an estimate $t^\star$ in the case of small amplitudes and a monochromatic forcing as

$$t^\star \approx \frac{hK^2d}{A\,\rho_{\text{eff}}\,\mathcal{C}^\ell_{\text{eff}}\,\omega_c} + \frac{1}{2f_c}. \tag{67}$$

Note that $t^\star$ decreases with d, as the smaller d is the stronger the non-linear effects are. The estimate (67) will be used in the ensuing examples as an upper bound on the duration of validity of the proposed effective models.

Remark 11. *In linear dynamical homogenization, it is known that the long-term behaviors of the microstructured wavefields are not well captured by effective models, in particular due to the dispersive nature of the former that develops with time, see e.g. [40, 22]. It is all the more so in the non-linear case as what can be qualified as* "long-term" *is directly correlated to the amplitude of the source, as discussed previously. The effective models derived in the present study are thus valid at relatively low source amplitudes and correspondingly short times. This issue will be illustrated in the numerical results below.*

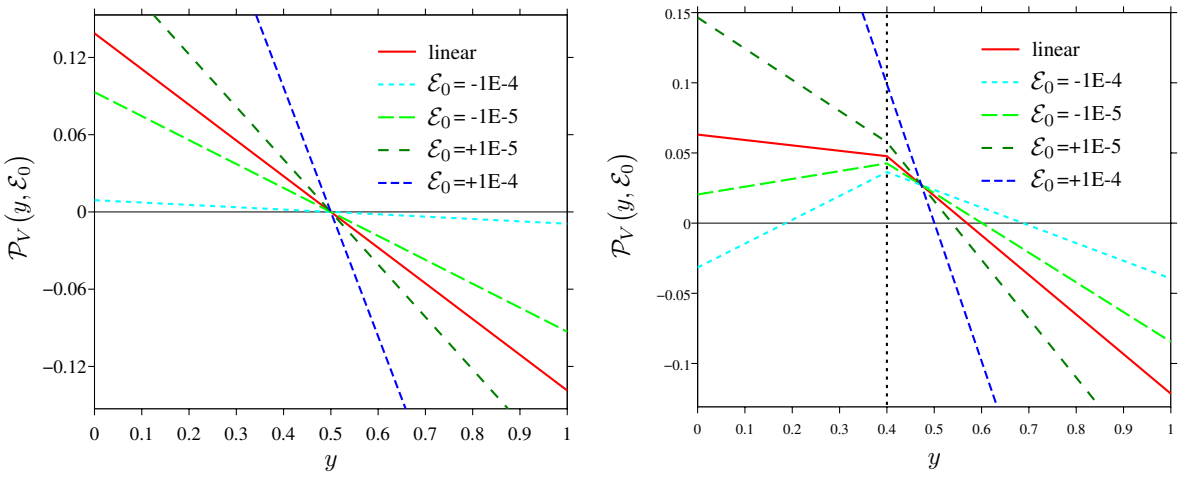

(a) Homogeneous periodic cell (Section 5.3)

(b) Bilaminated periodic cell (Section 5.4).

Figure 5: Velocity-based cell function $\mathcal{P}_V\big(y,\mathcal{E}_0(X,t)\big)$ in (66) for various strain amplitudes $\mathcal{E}_0$. The corresponding physical parameters are provided in the sections 5.3 and 5.4, respectively. In (b), the vertical dashed line indicates the position of the perfect interface between the two phases that constitute the bilaminated periodic cell.

5.2 Numerical set-up

5.2.1 Numerical schemes

In the following subsections, comparisons are made between full-field simulations in the microstructured configurations and simulations involving their homogenized counterparts (at the zeroth- and first-order). All the numerical simulations are based on a uniform grid, with space and time discretization parameters ΔX and Δt. A finite-volume scheme with flux limiters is implemented [27] both for the simulations in the microstructured configurations and in the homogenized ones. This non-linear scheme is of order 2 when the solution is sufficiently smooth, and it efficiently captures possible sharp wave-fronts in the microstructured configurations, as well as the shocks that can form in their homogenized counterparts.

For the microstructured configurations, the time step is adjusted based on the usual Courant-Friedrichs-Lewy (CFL) stability condition. The characteristic speeds being constant, so is Δt. Moreover, the interface transmission conditions (2) are handled using the so-called Explicit Simplified Interface Method, for technical details see [30] in the linear case and [31, 19, 20] in the non-linear one.

Concerning the homogenized models, the two hyperbolic systems (35) and (61) are solved sequentially, i.e. with $\Psi_0 = (\mathcal{E}_0, V_0)^\top$ being already computed when solving for $\overline{\Psi}_1 = (\overline{\mathcal{E}}_1, \overline{V}_1)^\top$, while the complete first-order approximation $U^{(1)}$ is computed afterwards by adding the corrector contribution as in (56) and (59). In addition, since the characteristic speeds $\nu_\pm$ depend non-linearly on the solution, see (65), then a time step Δt_n is computed at a given time iteration t_n so as to satisfy the CFL condition

$$\max_{X_j} \nu_+\big(\mathcal{E}_0(X_j,t_n)\big)\frac{\Delta t_n}{\Delta X} \leq 1,$$

where $\{X_j\}$ denotes the grid points.

The choice of the discretization parameter ΔX for the microstructured configurations is based on two criteria: (i) a sufficient number of computation points per wavelength; (ii) a sufficiently fine discretization of each cell in order to capture the fields evolving at the small scale. Given the aim of assessing the quality of the obtained effective models then criterion (ii) is the most penalizing: to

neglect the discretization effects then we typically consider 20 grid points in each cell, which leads, for the example considered below, to a number of grid points per wavelength at the central frequency of the order of 300, which is significantly oversampled in regard to (i). Note that, to illustrate the local effect of the first-order corrector, then the same discretization is employed here for the numerical simulations in the homogenized configurations.

CPU (s) / A	microstructured	homogenized
0.1	7.1	1.9
40	28.5	2.1
80	33.2	2.2

Table 1: CPU times for simulations in the microstructured and homogenized configurations.

Table 1 presents the CPU computation times measured for the numerical simulations associated with the figures 7–10. The simulations are performed on a single processor 3.6 GHz Intel Xeon PC. In the microstructured case, the CPU time depends strongly on the amplitude of the forcing. This is due to the discretization of the non-linear interface conditions in the immersed interface method employed here and that involves the resolution of non-linear systems with a Newton-Raphson scheme, see [31]. At low amplitudes, this resolution typically converges in 1 or 2 iterations. At higher amplitudes, the systems of equations become stiffer and finding a solution requires more iterations. In the mean time, the CPU time is almost independent of the forcing amplitude in the homogenized case. In practice, we could perfectly use a much coarser grid for the latter than that considered here. This, in turn, would significantly reduce the computation time and take full advantage of the effective models.

In the results presented hereafter, we will compare the velocity field V_h within the microstructured medium, with the velocity fields V_0 and $V^{(1)}$, which are associated with the zeroth- and first-order homogenized models, respectively. These quantities will be refereed to as the *microstructured* and *homogenized* fields, respectively.

5.2.2 Forcing

In dynamic homogenization, it is known that the validity of the effective models is subject to the smoothness of the initial data or of the source term, see e.g. [21]. Investigating these issues are beyond the scope of this study and we consider the initial data to be zero and an excitation by a smooth source term. The latter is defined as $F(X,t) = \delta(X - X_s)\, g(t)$, with X_s being a point lying in the computational domain and the time evolution $g(t)$ being chosen as the following combination of sinusoids with bounded support:

$$g(t) = \begin{cases} A \displaystyle\sum_{m=1}^{4} a_m \, \sin(\beta_m \, \omega_c \, t) & \text{if } 0 < t < \dfrac{1}{f_c}, \\ 0 \;\; \text{otherwise,} \end{cases} \tag{68}$$

where $\beta_m = 2^{m-1}$ and the coefficients a_m being $a_1 = 1$, $a_2 = -21/32$, $a_3 = 63/768$, $a_4 = -1/512$. It entails that $g \in C^6([0, +\infty[)$ and, so defined, $g(t)$ is a wide-band signal with a *central* frequency $f_c = \omega_c/2\pi$. The source temporal evolution $g(t)$ and its Fourier spectrum are displayed in Figure 6. Note that care is required to incorporate a localized source such as $F(X,t)$ defined above in the homogenized model [11].

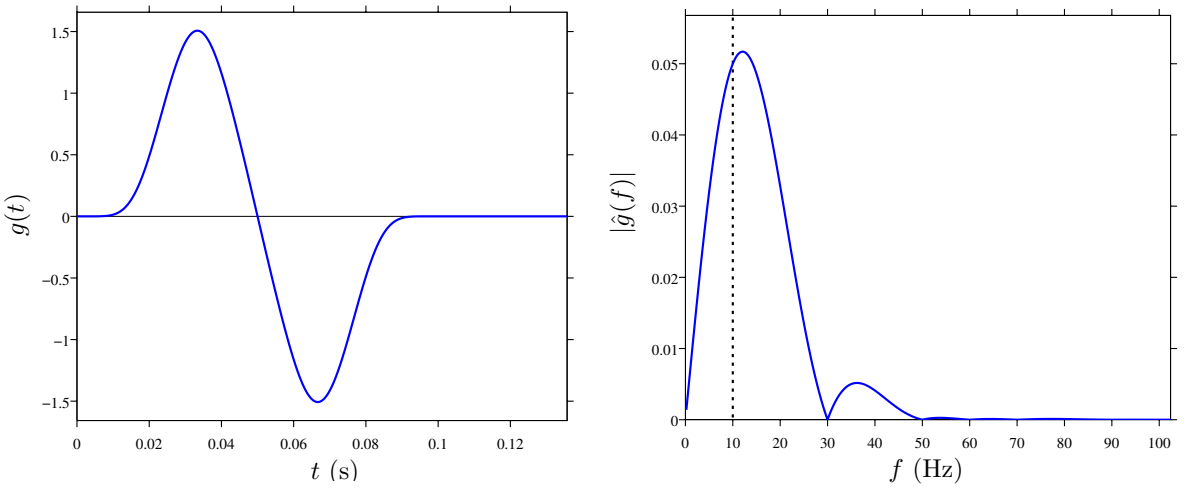

(a) Time evolution $g(t)$ of the source.

(b) Source spectrum, i.e. modulus of the Fourier transform $\hat{g}$. The vertical dotted line denotes f_c.

Figure 6: Source function (68) with amplitude $A = 1$ and central frequency $f_c = 10\,\mathrm{Hz}$.

5.3 Homogeneous periodic cell

5.3.1 Configuration

The computational domain considered is $[0,\, 1000]\,\mathrm{m}$, and it contains a number of interfaces with spacing $h = 10\,\mathrm{m}$. In the first configuration considered the periodic cell is homogeneous, with constant physical parameters $\rho = 1200\,\mathrm{kg/m^3}$ and $E = 9.408\cdot 10^9\,\mathrm{Pa}$. In (2b) and (6), the parameter characterizing the interfaces are $K = 2.45\cdot 10^9\,\mathrm{Pa/m}$ and $d = 10^{-4}\,\mathrm{m}$, respectively, while recall that $M = 0\,\mathrm{Pa.s^2/m}$. The corresponding value of the effective parameters are $\rho_{\mathrm{eff}} = 1200\,\mathrm{kg/m^3}$ and $\mathcal{C}^{\ell}_{\mathrm{eff}} = 6.79\cdot 10^9\,\mathrm{Pa}$. The associated velocity-based cell function $\mathcal{P}_V$ in (66) is displayed in Figure 5a.

Moreover, the source F is defined with $X_s = 505\,\mathrm{m}$, i.e. at the center of a cell, and the simulations are stopped before the domain boundaries are reached. Note also that, in the hyperbolic system (61) for $\overline{\Psi}_1$, the source term $\mathbb{S}(\Psi_0)$ vanishes in the case considered, as $\mathcal{S}(U_0) = 0$ when the periodic cell is homogeneous according to Property 5. Lastly, given the chosen source signal (68), we define the parameter η relatively to the central frequency f_c, i.e. $\eta = \omega_c\, h/\nu^{\ell}_{+}$, with ν^{ℓ}_{+} being the characteristic wave speed defined in Remark 10.

5.3.2 Numerical results

Comparisons between microstructured and homogenized fields. Figure 7 corresponds to an excitation at the central frequency $f_c = 10\,\mathrm{Hz}$, associated with the value $\eta = 0.26$, and amplitude $A = 0.1$. Snapshots of the velocity fields at $t = 0.16\,\mathrm{s}$ are provided for both the microstructured medium and the homogenized model. A close-up on the right-going wave highlights the excellent agreement between the associated fields V_h and $V^{(1)}$. The extra zoomed-in Figure 7d shows that, at the scale of the microstructure, the local fluctuations of V_h are correctly captured by the first-order corrector, contrary to the zeroth-order effective field, as expected. Figure 8 corresponds to the same numerical experiment as in Fig. 7 but with the larger forcing amplitude $A = 40$. Although non-linear effects are now being fully solicited, the same conclusions are reached with an excellent agreement between V_h and $V^{(1)}$, even at the microscale compared to V_0.

For the given amplitude value $A = 40$, Figure 9 now illustrates the influence of the wavelength by considering relatively larger values of the parameter η. Close-ups are centered on the right-going

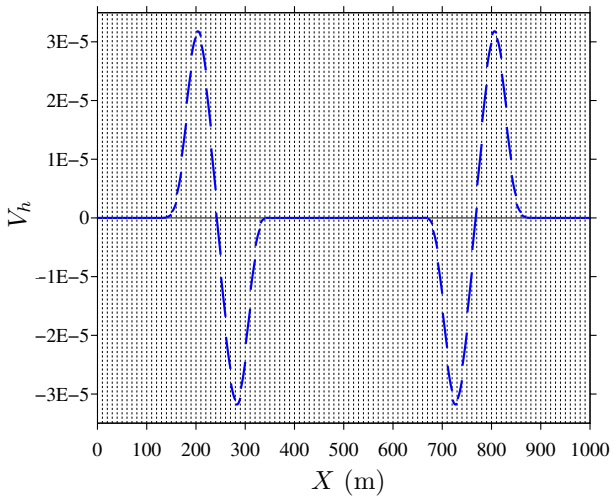

(a) Field V_h in the microstructured medium.

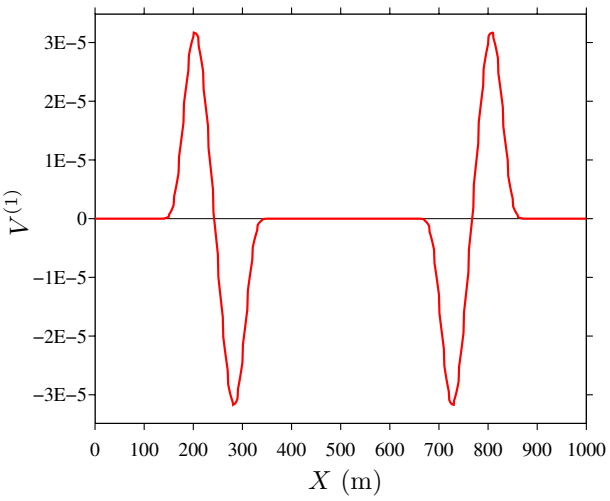

(b) First-order homogenized field $V^{(1)}$.

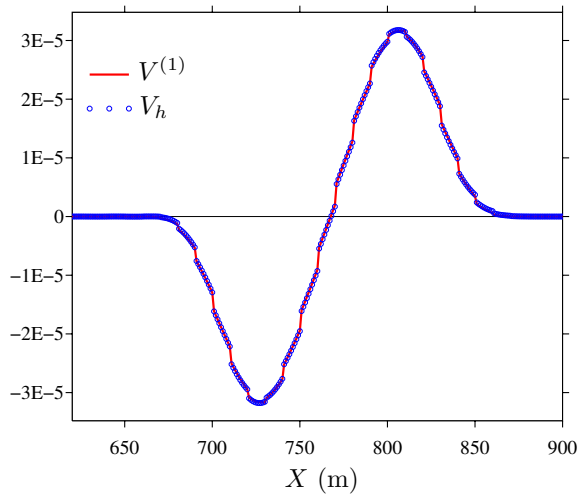

(c) Superposition of the fields V_h and $V^{(1)}$.

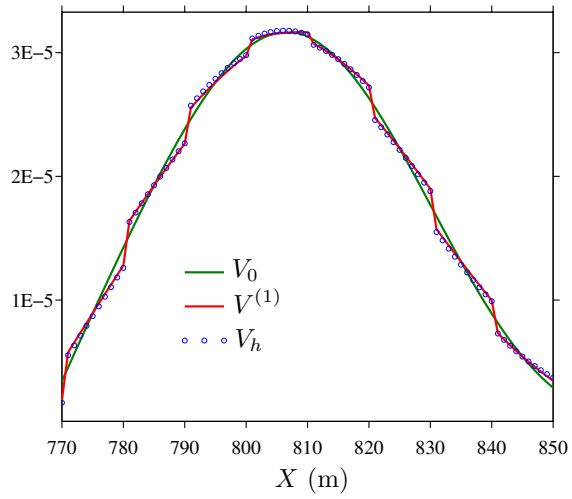

(d) Close-up showing the zeroth- and first-order homogenized fields V_0 and $V^{(1)}$, respectively, and V_h.

Figure 7: Snapshots of the velocity fields (in m/s) at $t = 0.16\,\mathrm{s}$ in the case of a homogeneous periodic cell and an excitation by a pulse with central frequency $f_c = 10\,\mathrm{Hz}$ (so that $\eta = 0.26$) and amplitude $A = 0.1$.

wave and show a comparison between the homogenized wavefield $V^{(1)}$ and the microstructured one V_h. At $f_c = 15\,\mathrm{Hz}$ (i.e. $\eta = 0.39$) then, on the one hand, the first-order corrector is still able to capture adequately the main wavefield variations within the microstructure, see Fig. 9a. On the other hand, the field V_h exhibits high-frequency oscillations after the passing of the main front, and computations on finer grids have confirmed that these oscillations are not numerical artifacts but a physical phenomenon, which is typical of a dispersive effect. As such, these cannot be captured by the first-order homogenized model that is intrinsically non-dispersive. At the higher frequency $f_c = 20\,\mathrm{Hz}$ (i.e. $\eta = 0.52$) in Fig. 9b the agreement between V_h and $V^{(1)}$ is deteriorating, as expected, and dispersive effects also amplify within the microstructure.

Figure 10 illustrate another limitation of the proposed effective model that is the implicit assumption of a relatively low source amplitude. The central frequency is kept as in the figures 7 and 8, i.e. $f_c = 10\,\mathrm{Hz}$ so that $\eta = 0.26$, but the source amplitude is now increased to $A = 60$ and $A = 120$. As A increases, the stiffening of the fronts becomes more apparent. Moreover, the dispersive

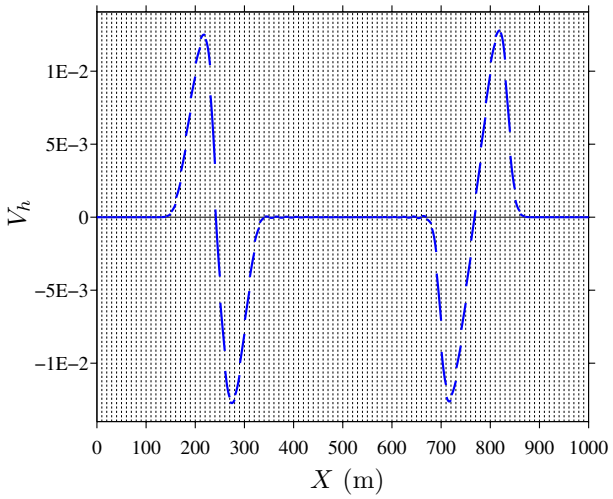

(a) Field V_h in the microstructured medium.

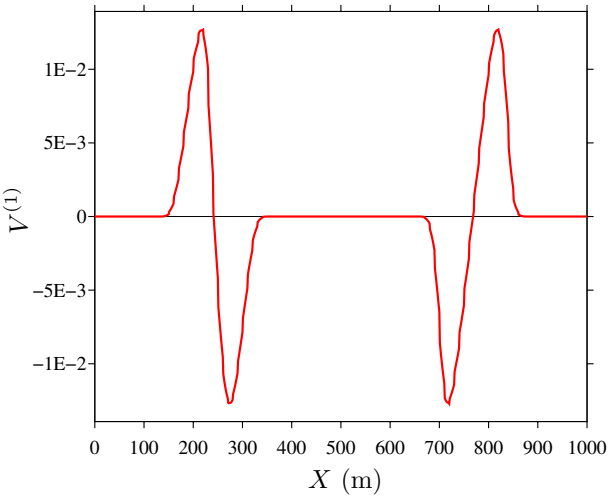

(b) First-order homogenized field $V^{(1)}$.

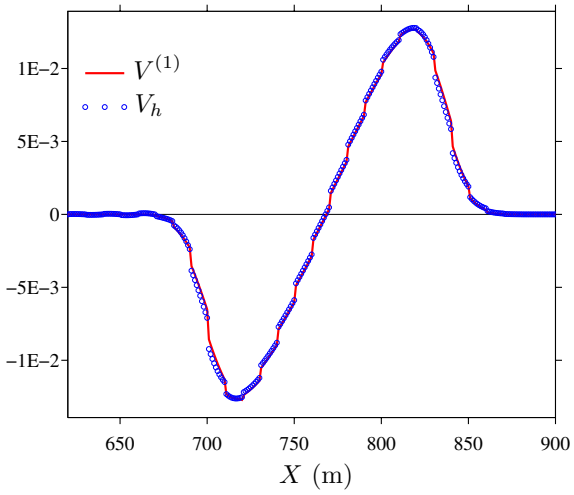

(c) Superposition of the fields V_h and $V^{(1)}$.

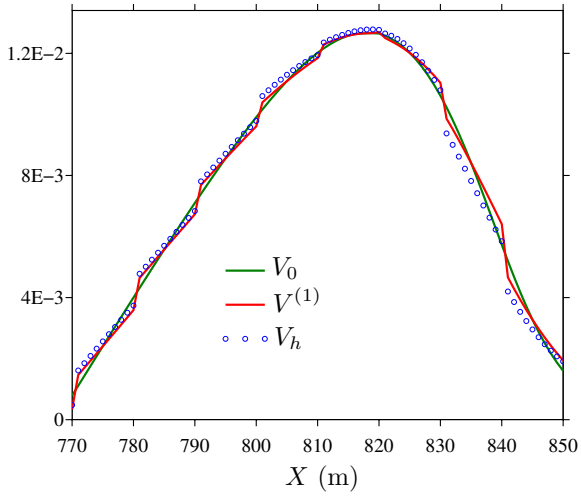

(d) Close-up showing the zeroth- and first-order homogenized fields V_0 and $V^{(1)}$, respectively, and V_h.

Figure 8: Snapshots of the velocity fields (in m/s) at $t = 0.16\,\mathrm{s}$ in the case of a homogeneous periodic cell and an excitation by a pulse with central frequency $f_c = 10\,\mathrm{Hz}$ (i.e. $\eta = 0.26$) and amplitude $A = 40$.

high-frequency oscillations within the microstructure also increase while they are not captured by the homogenized model, as previously underlined. More importantly, as the source amplitude increases, the validity of the former cannot be guaranteed as we find ourselves beyond the assumptions used in the asymptotic analysis, see Remark 3. Note finally, that for the values considered of the amplitude, i.e. $A = 0.1$, 40, 60, 80 and 120, then the maximum magnitudes of the strain field $\mathcal{E}_0$ in the zeroth-order homogenized model are $1.35{\cdot}10^{-8}$, $5.5{\cdot}10^{-6}$, $8.4{\cdot}10^{-6}$, $1.15{\cdot}10^{-5}$ and $1.7{\cdot}10^{-5}$, respectively, at $t = 0.16\,\mathrm{s}$. By reference to the effective stress-strain relation $\mathcal{G}_{\mathrm{eff}}$ plotted in Figure 4a, these strain values appear to be relatively low.

Generation of harmonics. In the original microstructured medium, the presence of non-linear imperfect interfaces generate harmonics of a given source signal. The calculation of their amplitudes has been performed in [29] in the case of a single interface, while the theoretical analysis of the case considered here of an array of interfaces is much more involved and is beyond the scope of the

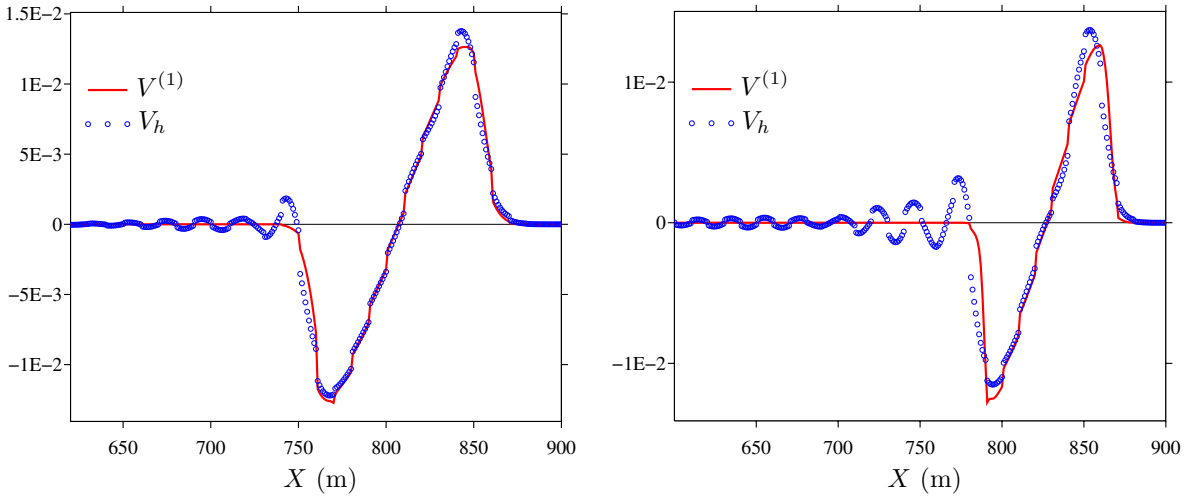

(a) $f_c = 15\,\text{Hz}$ (i.e. $\eta = 0.39$) **(b)** $f_c = 20\,\text{Hz}$ (i.e. $\eta = 0.52$)

Figure 9: Superposition of the fields V_h and $V^{(1)}$ (in m/s) at $t = 0.16\,\text{s}$ with close-up on the right-going waves in the case of a homogeneous periodic cell and a source of amplitude $A = 40$, for two different central frequencies.

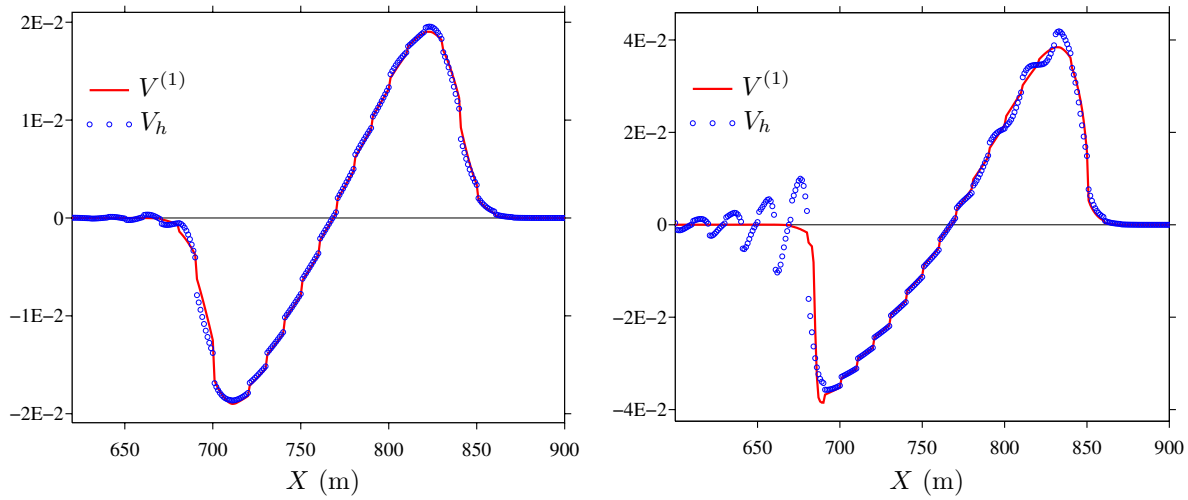

(a) $A = 60$. **(b)** $A = 120$.

Figure 10: Superposition of the fields V_h and $V^{(1)}$ (in m/s) at $t = 0.16\,\text{s}$ with close-up on the right-going waves in the case of a homogeneous periodic cell and a source at central frequency $f_c = 10\,\text{Hz}$ (i.e. $\eta = 0.26$), for two different amplitudes.

present study. Yet, we compare here numerically these harmonics with those generated when using the *zeroth-order* effective model, which is itself non-linear.

For this purpose, we consider simulations both in the microstructured and homogenized media, with a receiver positioned at $X_r = 805\,\text{m}$ (at the center of a cell) that records the velocity fields V_h and V_0, respectively. The source is monochromatic, i.e. such that $a_m = 0$ for all $m > 1$ in (68) and with central frequency $f_c = 10\,\text{Hz}$, and the wavefields are recorded once their time evolution has reached a steady-state at X_r. Note that the computational domain is adapted in these simulations to avoid being polluted by reflections from the boundaries. Finally, the discrete Fourier transforms of the

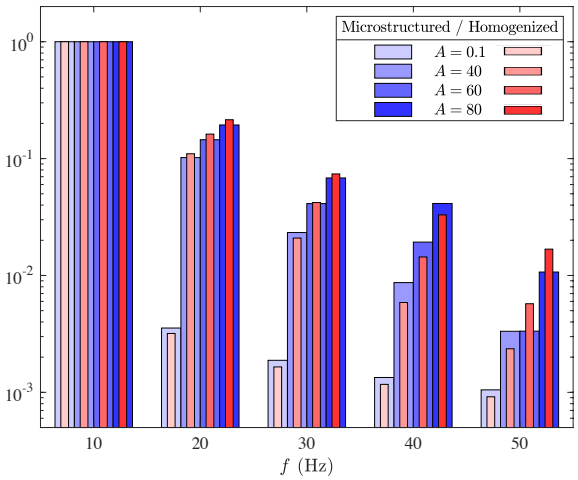

Figure 11: Amplitude of the normalized Fourier coefficients of the fields V_h (in blue, thick bars) and V_0 (in red, thin bars) recorded at $X_r = 805\,\mathrm{m}$ in the case of a homogeneous periodic cell and a monochromatic forcing at $f_c = 10\,\mathrm{Hz}$ with a varying amplitude A.

acquired signals are computed and Figure 11 shows in logarithmic scale the normalized amplitude of the Fourier coefficients for different forcing amplitudes. When $A = 0.1$ the amplitude of the harmonics are relatively low. For the higher amplitudes considered, i.e. $A = 40$, 60 and 80, then the amplitudes of the multiple harmonics increase, as expected, which generate stronger non-linear effects as previously underlined. The main observation here is that there is an overall satisfying agreement between the amplitude of the harmonics generated using the microstructured model (in blue, thick bars) compared to its zeroth-order effective counterpart (in red, thin bars).

Formation of shocks. The energy analyses of the microstructured and of the effective zeroth-order models have been performed in the sections 2.3 and 3.3.2, respectively. Moreover, it has been discussed in Section 5.1 that the homogenized model allows the formation of shocks in a finite time, unlike the microstructured media, and a corresponding estimated time $t^\star$ has been proposed.

This discussion is now illustrated numerically in Figure 12. The computational domain is $[0,\ 2000]\,\mathrm{m}$ and a source with central frequency $f_c = 10\,\mathrm{Hz}$ and amplitude $A = 40$ (left column) or $A = 60$ (right column) is placed at $X_s = 1010\,\mathrm{m}$, i.e. at the center of a cell. The top (resp. middle) panels correspond to seismograms of the velocity field V_h (resp. V_0). The bottom panels show the temporal evolutions of the energies in the microstructured medium and in the homogenized one, i.e. $\mathscr{E}_h$ and $\mathscr{E}_0$ respectively. In each case, the dotted lines denote the estimated time $t^\star$ in (67). For $t < t^*$ both the wavefields and their energies agree well. At about $t = t^\star$, the effective energy $\mathscr{E}_0$ starts to decrease, which is typical of a shock formation, as can be observed in Fig. 12c and 12d. In the mean time, the energy $\mathscr{E}_h$ in the microstructured media is conserved, as expected. Dispersive effects are again clearly visible in Fig.12a and 12b, i.e. high-frequency oscillations, which somehow *regularize* the wavefield that propagates within the microstructured medium and prevent the formation of shocks.

Figure 13 illustrates the influence of the shocks on the spectral content of the waves. Considering the configuration of Figure 12 then, to do so, two receivers are placed at $X_{r1} = 1205\,\mathrm{m}$ and $X_{r2} = 1705\,\mathrm{m}$, i.e. both at the center of a cell near the source and further away. The propagation distance at X_{r1} (resp. X_{r2}) is about one (resp. three) wavelength relatively to the central frequency f_c. Figure 13 then represents the discrete Fourier spectra of the recorded time-domain signals for the two forcing amplitudes $A = 40$ and $A = 60$ considered. The waves reach the receiver X_{r1} before the time $t^\star$, so that no shock has formed yet in the homogenized media. We then note a satisfying agreement between the microstructured and the effective spectra at low frequency, see Fig. 13a and 13b. When

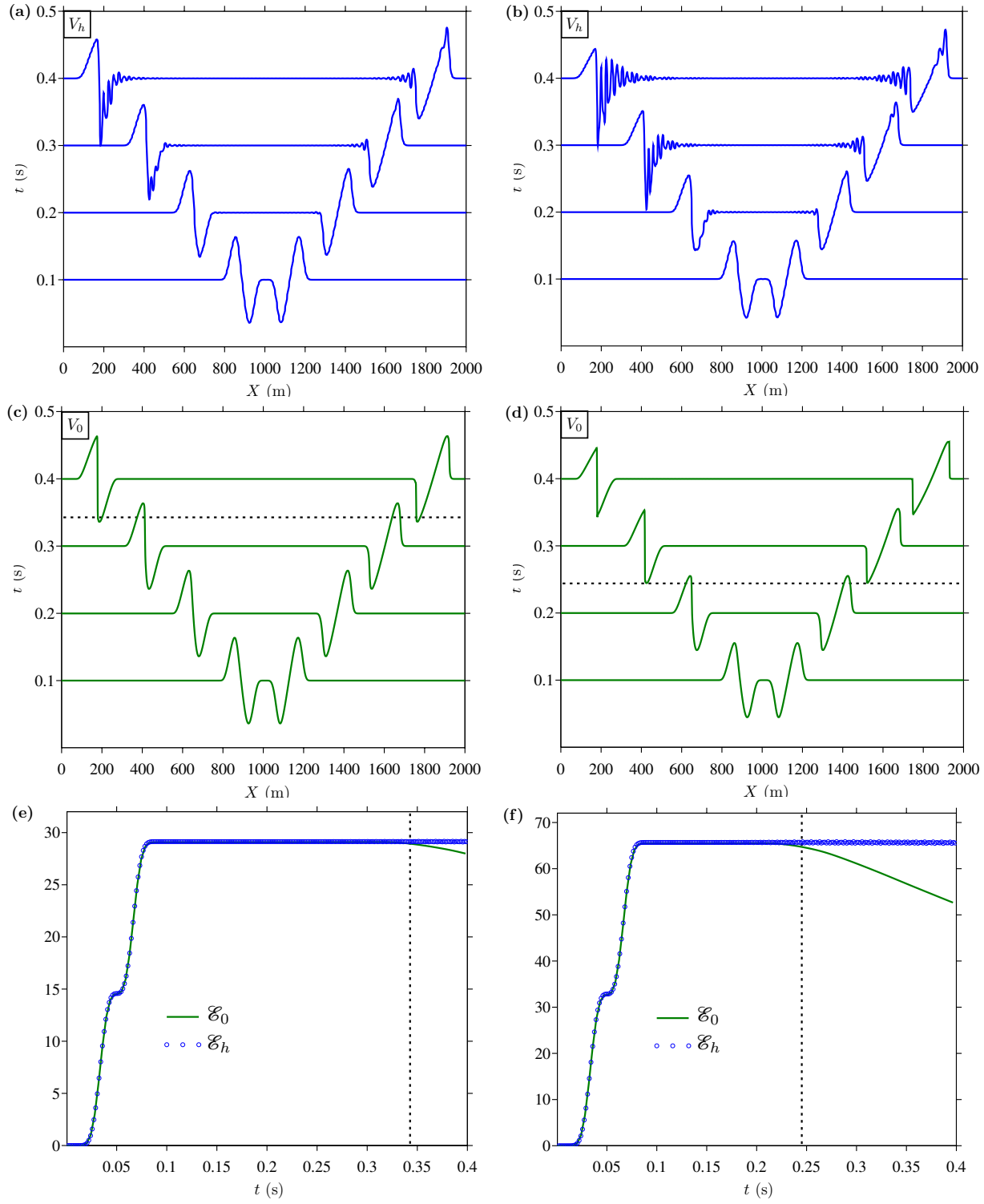

Figure 12: Case of a homogeneous periodic cell and an excitation by a pulse centered at $f_c = 10\,\text{Hz}$ with amplitude $A = 40$ (left panels) and $A = 60$ (right panels). Top: seismograms of V_h in the microstructured medium. Middle: seismograms of the homogenized field V_0. Bottom: superposition and time evolution of the energies $\mathscr{E}_h$ and $\mathscr{E}_0$. The dotted lines denote the estimated time $t^\star$ in (67) for each case.

recorded at the receiver X_{r2}, the wavefield V_0 has now formed a shock while V_h is characterized by stronger dispersive effects, as previously observed. Accordingly, we notice significant enrichments of

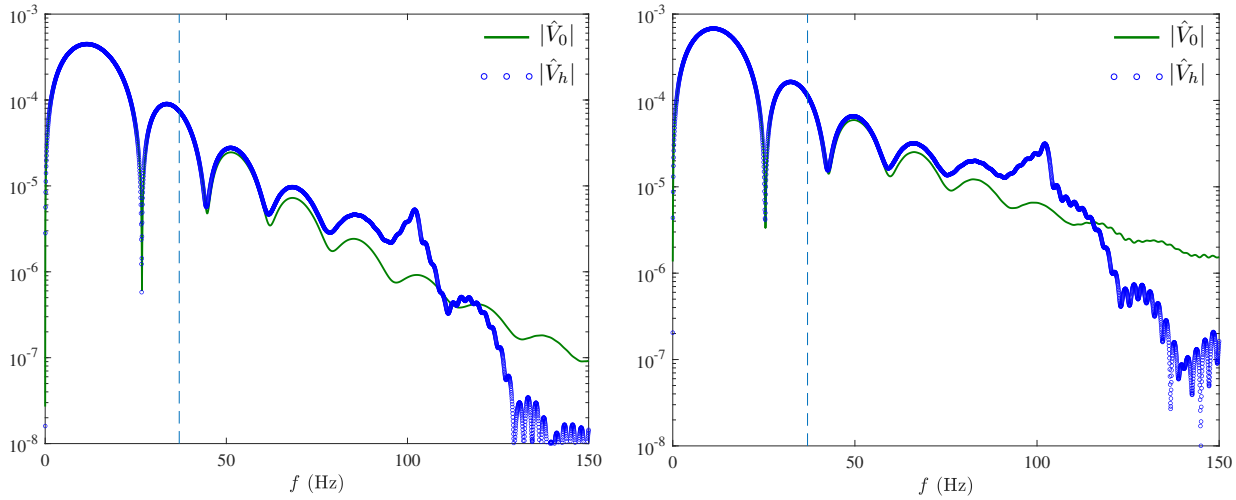

(a) $A = 40$ and X_{r1}.

(b) $A = 60$ and X_{r1}.

(c) $A = 40$ and X_{r2}.

(d) $A = 60$ and X_{r2}.

Figure 13: Case of a homogeneous periodic cell and an excitation by a pulse centered at $f_c = 10\,\text{Hz}$ with amplitude $A = 40$ (left panels) and $A = 60$ (right panels), as in Figure 12. Spectra of the velocity fields V_h and V_0 recorded at two receivers placed at $X_{r1} = 1205\,\text{m}$ and $X_{r2} = 1705\,\text{m}$. The vertical dashed line indicates the value of the frequency that corresponds to $\eta = 1$.

the associated spectra, see Fig. 13c and 13d. In particular, those associated with V_0 now behave as sinc functions, which is characteristic of the Fourier transforms of discontinuous functions. While at frequencies $f \geq 37\,\text{Hz}$, which corresponds to $\eta = 1$, the Fourier contents associated with these two models are clearly different, they still agree relatively well for lower frequencies $f \leq 37\,\text{Hz}$.

Remark 12. *The analysis of this paragraph pertains to the zeroth-order homogenized model. Yet, as it can be seen from the figures 9b and 10b, shocks can also develop in a finite time with the first-order model. The associated corrector is indeed not able to capture high-frequency dispersive effects, see also Remark 11.*

5.4 Bilaminated periodic cell

5.4.1 Configuration

In a second example, we consider the case of a bilaminated periodic cell, a configuration which has been studied in [10] in the case of perfect interfaces. A motivation for this second example is that, in the hyperbolic system (61) for $\overline{\Psi}_1$, the source term $\mathbb{S}(\Psi_0)$ is now non-zero, see Property 5, contrary to the case considered previously where the periodic cell was homogeneous.

The domain is kept as $[0,\, 1000]\,\mathrm{m}$ and it contains a set of imperfect interfaces with spacing $h = 20\,\mathrm{m}$. Between two interfaces, the periodic cell is composed of two homogeneous elastic phases, respectively of length $h_1 = 8\,\mathrm{m}$ and $h_2 = 12\,\mathrm{m}$ and of constitutive parameters $\rho_1 = 1200\,\mathrm{kg/m^3}$, $E_1 = 9.408{\cdot}10^9\,\mathrm{Pa}$ and $\rho_2 = 1400\,\mathrm{kg/m^3}$, $E_2 = 1.26{\cdot}10^{10}\,\mathrm{Pa}$. On the one hand, the interface between the two phases within each cell is assumed to be perfect. On the other hand, the interfaces that bound each cell are imperfect, with $K = 2.45{\cdot}10^9\,\mathrm{Pa/m}$ and $d = 10^{-4}\,\mathrm{m}$, while $M = 0\ \mathrm{Pa.s^2/m}$, as in the homogeneous case of Section 5.3. The corresponding values of the effective coefficients are $\rho_{\text{eff}} = 1320\,\mathrm{kg/m^3}$ and $\mathcal{C}^{\ell}_{\text{eff}} = 9.0462\cdot 10^9\,\mathrm{Pa}$, and the associated velocity-based cell function $\mathcal{P}_V$ is displayed in Figure 5b. Lastly, the parameter η is defined as in Section 5.3 as $\eta = \omega_c\, h/\nu^{\ell}_{+}$, with ν^{ℓ}_{+} given in Remark 10.

5.4.2 Numerical results

Figure 14 is analogous to the figures 7 and 8 and corresponds to an excitation at the central frequency $f_c = 5\,\mathrm{Hz}$, so that $\eta = 0.24$, and with amplitude $A = 40$. Snapshots of the microstructured velocity fields V_h and its effective counterparts V_0 and $V^{(1)}$ are displayed at time $t = 0.2\,\mathrm{s}$. For such a configuration, and as in the previous one, these numerical results highlight the excellent agreement of the effective models, which capture both the main variations of V_h and its local fluctuations at the scale of the microstructure. The source term $\mathbb{S}(\Psi_0)$ is thus properly handled numerically.

On Figure 15 we illustrate that, as expected, the validity of the effective models deteriorates as the forcing amplitude increases. In these examples, the source central frequency is kept as in Figure 14, i.e. $f_c = 5\,\mathrm{Hz}$ (i.e. $\eta = 0.24$), but the source amplitude is increased to $A = 120$ and $A = 200$. For such amplitudes, the dispersive effects and the distortion of the microstructured wave-fronts are stronger. The macroscopic wave motion is still relatively well captured but not the small-scale microstructured wavefield fluctuations. Note finally that for the values considered of the amplitude in these examples, i.e. $A = 40$, 120 and 200, then the maximum magnitudes of the strain field $\mathcal{E}_0$ in the zeroth-order homogenized model are $4.8\cdot 10^{-6}$, $1.55\cdot 10^{-5}$ and $3\cdot 10^{-5}$, respectively, at $t = 0.2\,\mathrm{s}$. The first two strain maxima are relatively low values given the effective stress-strain relation $\mathcal{G}_{\text{eff}}$ of the considered configuration but the third one is rather not.

6 Conclusion

The propagation of transient elastic waves in a 1D periodic array, characterized by linear elastic cells bonded by non-linear interfaces, has been investigated in the long-wavelength regime using the two-scale homogenization method. Considering a generic non-linear interface law, subject to certain appropriate requirements, and limiting ourselves to low-amplitude forcings, then a first-order approximation of the microstructured wavefield has been derived. The main findings of the present study can then be summarized as follows:

1. The microstructured problem is associated with an energy $\mathscr{E}_h$, with bulk and interface contributions, which is conserved over time in the absence of external sources.

2. The wavefield U_h is characterized by a spectral content that enriches over time and with the amplitude of the forcing. In other words, dispersive effects increase and wave-fronts sharpen all

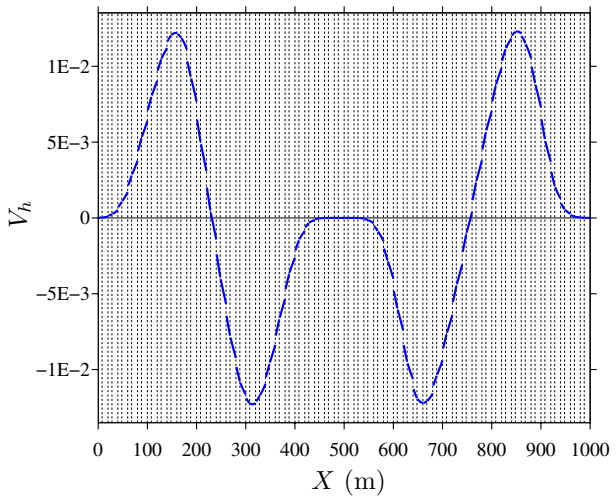

(a) Field V_h in the microstructured medium.

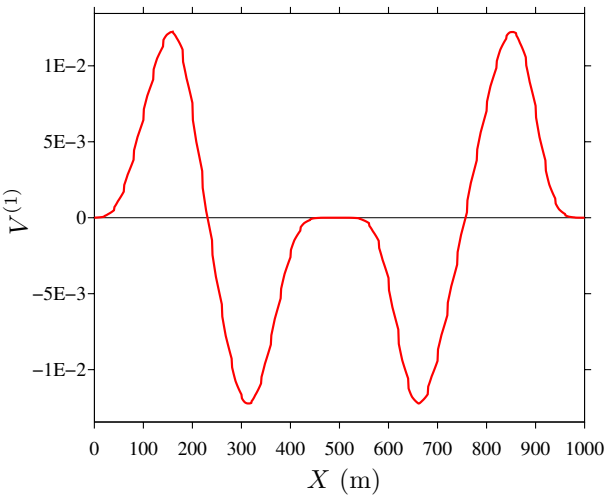

(b) First-order homogenized field $V^{(1)}$.

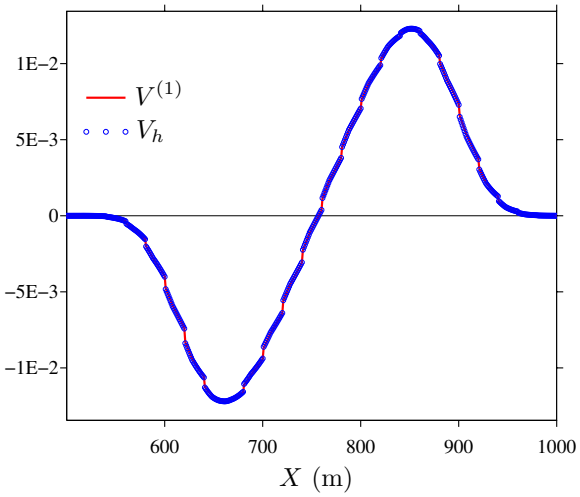

(c) Superposition of the fields V_h and $V^{(1)}$.

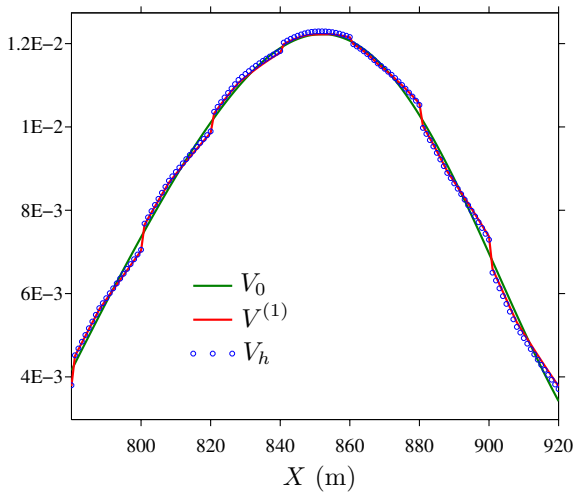

(d) Close-up showing the zeroth- and first-order homogenized fields V_0 and $V^{(1)}$, respectively, and V_h.

Figure 14: Snapshots of the velocity fields at $t = 0.2\,\mathrm{s}$ in the case of a bilaminated periodic cell and an excitation by a pulse with central frequency $f_c = 5\,\mathrm{Hz}$ so that $\eta = 0.24$ and amplitude $A = 40$.

the more that the observation time or the amplitude of the source increase.

3. The two-scale homogenization method is deployed, up to the first-order, relatively to the small geometrical parameter η only. In particular, the amplitude of the source is assumed in the analysis to not scale with η, which restrains us to the case of sources of relatively low amplitude.

4. The zeroth-order contribution to U_h is a mean field U_0 that is solution of a wave equation with a non-linear constitutive stress-strain relation.

5. The governing equations for U_0 can be recast in the form of a non-linear and strictly hyperbolic first-order system for the strain-velocity variable $\Psi_0 = (\mathcal{E}_0, V_0)^\top$.

6. The non-linearity of the obtained hyperbolic system allows the formation of shocks in a finite time and a corresponding estimation $t^\star$ is provided.

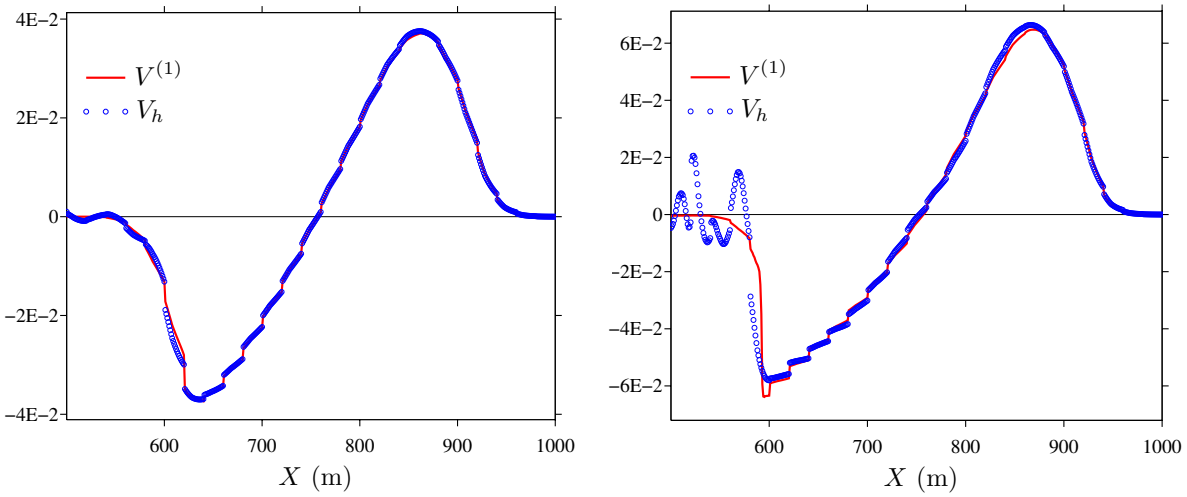

(a) $A = 120$. **(b)** $A = 200$.

Figure 15: Superposition of the fields V_h and $V^{(1)}$ at $t = 0.2\,\mathrm{s}$ with close-up on the right-going waves in the case of a homogeneous periodic cell and a source at central frequency $f_c = 5\,\mathrm{Hz}$ (i.e. $\eta = 0.24$), for two different amplitudes.

7. The associated macroscopic energy $\mathscr{E}_0$ is conserved, in the absence of external source, as long as shocks do not appear. The model for U_0 is a meaningful effective one for U_h for times, at most, such that $t < t^\star$.

8. In the numerical examples considered, U_0 approximates well the macroscopic behavior of U_h spatially. In the Fourier space, the low frequency contents of both fields agree well, even for times $t > t^\star$.

9. The first-order corrector term U_1 for U_h is expressed in terms of a cell function $\mathcal{P}$ and a mean field $\overline{U}_1$ that is solution of a wave equation. Without further assumptions, both $\mathcal{P}$ and the constitutive relation for $\overline{U}_1$ and its source term depend non-linearly on U_0.

10. The equation for $\overline{U}_1$ can be recast as a linear and strictly hyperbolic first-order system on the strain-velocity variable $\overline{\Psi}_1 = (\overline{\mathcal{E}}_1, \overline{V}_1)^\top$, whose characteristic speeds are equal to those of the system for Ψ_0.

11. In the numerical examples considered, the field $U^{(1)} = U_0 + hU_1$ provides a satisfying approximation of U_h, up to the fluctuations of the latter at the scale of the microstructure.

12. The dispersive behavior of U_h is not captured by the proposed effective models. Moreover, as expected, the approximation quality of the latter decreases as the observation time or the source amplitude increase.

Overall, the present work has led to effective models, in the time-domain, for approximating waves in a 1D non-linear media. The 1D setting considered is somehow particular in that it might not be straightforward to extend some parts, such as the explicit derivation of the cell function, of the adopted approach in higher dimensions. Nevertheless, the presented numerical results highlight the usefulness of the proposed effective models. A number of questions remain opened and among possible future developments, it seems important to us to be able to capture the dispersive behavior of the microstructured wavefield. This might be possible by deploying the current homogenization method, with one time-scale and two length-scales, up to at least the second order. Introducing a slow and

a fast time-scales in the asymptotics is also worth considering in this prospect. Deriving an effective model for waves of relatively larger amplitudes would also be interesting, as we have shown that non-linear phenomena are strongly dependent on the source amplitude. To do so, it might be necessary to consider an additional scaling parameter and its relation to the geometrical parameter η, which would correspondingly yield a specific model.

A Proof of Property 1

To prove Property 1, the equation (1) is multiplied by V_h and integrated by parts on I. Omitting the space and time variable for conciseness, it leads to

$$\int_I \rho_h \frac{\partial V_h}{\partial t} V_h \,\mathrm{d}X = \Big[\Sigma_h(\cdot,t)V_h(\cdot,t)\Big]_a^b - \sum_{X_n^I} [\![\Sigma_h V_h]\!]_{X_n^I} + \int_I \left\{ F V_h - \Sigma_h \frac{\partial V_h}{\partial X} \right\} \mathrm{d}X. \tag{69}$$

Now, focusing on the jump term at X_n^I, we write

$$[\![\Sigma_h V_h]\!]_{X_n^I} = [\![\Sigma_h]\!]_{X_n^I} \langle\!\langle V_h \rangle\!\rangle_{X_n^I} + \langle\!\langle \Sigma_h \rangle\!\rangle_{X_n^I} [\![V_h]\!]_{X_n^I},$$

which owing to the interface conditions (2) is recast as

$$[\![\Sigma_h V_h]\!]_{X_n^I} = M \langle\!\langle V_h \rangle\!\rangle_{X_n^I} \left\langle\!\!\left\langle \frac{\partial V_h}{\partial t} \right\rangle\!\!\right\rangle_{X_n^I} + K\,\mathcal{R}\left([\![U_h]\!]_{X_n^I}\right) \left[\!\!\left[\frac{\partial U_h}{\partial t} \right]\!\!\right]_{X_n^I}. \tag{70}$$

We assume that the displacement field is sufficiently smooth in time so that, for $W = U_h$ or V_h, it holds

$$\left[\!\!\left[\frac{\partial W}{\partial t} \right]\!\!\right]_{X_n^I} = \frac{\mathrm{d}}{\mathrm{d}t} [\![W]\!]_{X_n^I} \qquad \text{and} \qquad \left\langle\!\!\left\langle \frac{\partial W}{\partial t} \right\rangle\!\!\right\rangle_{X_n^I} = \frac{\mathrm{d}}{\mathrm{d}t} \langle\!\langle W \rangle\!\rangle_{X_n^I}. \tag{71}$$

Moreover, we have the following identity

$$K\,\mathcal{R}\left([\![U_h]\!]_{X_n}\right) \frac{\mathrm{d}}{\mathrm{d}t} [\![U_h]\!]_{X_n^I} = \frac{\mathrm{d}}{\mathrm{d}t} K \int_c^{[\![U_h]\!]_{X_n^I}} \mathcal{R}(\zeta)\,\mathrm{d}\zeta, \tag{72}$$

where c is a constant for the time variable. For definiteness of the energy, we set $c = 0$. Making use of (71) and (72) in (70) and inserting that back in (69) finally leads to

$$\frac{\mathrm{d}}{\mathrm{d}t} \frac{1}{2} \int_I \left\{ \rho_h V_h^2 + \frac{1}{E_h} \Sigma_h^2 \right\} \mathrm{d}X + \frac{\mathrm{d}}{\mathrm{d}t} \sum_{X_n^I} \left\{ \frac{1}{2} M \langle\!\langle V_h \rangle\!\rangle_{X_n^I}^2 + K \int_0^{[\![U_h]\!]_{X_n^I}} \mathcal{R}(\zeta)\,\mathrm{d}\zeta \right\} - \Big[\Sigma_h(\cdot,t)V_h(\cdot,t)\Big]_a^b = \int_I F V_h \,\mathrm{d}X.$$

Using the notation of Definition 1 and introducing $C(t) = -\big[\Sigma_h(\cdot,t)V_h(\cdot,t)\big]_a^b$, then the previous equation can be recast as

$$\frac{\mathrm{d}}{\mathrm{d}t}(\mathscr{E}_h^m + \mathscr{E}_h^i) + C(t) = \int_I F V_h \,\mathrm{d}X. \tag{73}$$

Provided that V_h and Σ_h are compactly supported at $t = 0$ and if the domain I is sufficiently large then $C(t) = 0$. Therefore, owing to (73), if $F = 0$ we get $\dfrac{\mathrm{d}}{\mathrm{d}t}(\mathscr{E}_h^m + \mathscr{E}_h^i) = 0$.

Furthermore, according to Assumptions 1 we have that each term in (8a) is positive so that $\mathscr{E}_h^m(t) \geq 0$. From Assumptions 2 we also have

$$\int_0^{[\![U_h]\!]_{X_n^I}} \mathcal{R}(\zeta)\,\mathrm{d}\zeta = \int_0^{[\![U_h]\!]_{X_n^I}} \int_0^{\zeta} \mathcal{R}'(\xi)\,\mathrm{d}\xi\,\mathrm{d}\zeta \geq \mathcal{R}'_{\min} \frac{[\![U_h]\!]_{X_n^I}^2}{2} \geq 0, \tag{74}$$

given that $\mathcal{R}'(\xi) \geq \mathcal{R}'_{\min} > 0$ on the interval $\left[0, [\![U_h]\!]_{X_n^I}\right]$. Therefore, each term in (8b) is positive and thus $\mathscr{E}_h^i(t) \geq 0$. Finally, we recover explicitly the quantity $\mathscr{E}_h^i$ in Definition 1 by noting that, from (2), we have $[\![U_h]\!]_{X_n^I} = \mathcal{R}^{-1}(\langle\!\langle \Sigma_h(\cdot,t) \rangle\!\rangle_{X_n^I}/K)$.

Lastly, if $(\mathscr{E}_h^m + \mathscr{E}_h^i) = 0$ then $\mathscr{E}_h^m = 0$ hence $V_h = 0$ and $\Sigma_h = 0$ almost everywhere in I. Moreover, we have $\mathscr{E}_h^i = 0$, which on the one hand implies that $\langle\!\langle V_h \rangle\!\rangle_{X_n^I} = 0$ and $[\![\Sigma_h]\!]_{X_n^I} = 0$. On the other hand we also have $[\![U_h]\!]_{X_n^I} = 0$ from (74), which implies in turn that $[\![V_h]\!]_{X_n^I} = 0$ and $\langle\!\langle \Sigma_h \rangle\!\rangle_{X_n^I} = 0$. As a consequence, both V_h and Σ_h vanish on I.

B Proof of Property 3

In this whole proof, the manipulated fields are assumed to be sufficiently regular, typically, differentiable. Similarly to the proof in Appendix A, the equation (30) is multiplied by V_0 and integrated by parts on $I = [a, b]$ as

$$\begin{aligned} \int_I \rho_{\text{eff}} \frac{\partial V_0}{\partial t} V_0 \, \mathrm{d}X &= \int_I \left\{ \frac{\partial \Sigma_0}{\partial X} + F \right\} V_0 \, \mathrm{d}X, \\ &= \Big[\Sigma_0(\cdot,t) V_0(\cdot,t) \Big]_a^b + \int_I \left\{ F V_0 - \Sigma_0 \frac{\partial V_0}{\partial X} \right\} \mathrm{d}X. \end{aligned} \tag{75}$$

We now focus on the third right-hand side term in the equation above. Noticing that $\partial V_0/\partial X = \partial \mathcal{E}_0/\partial t$ and using the effective strain-stress relation we get

$$\int_I \Sigma_0 \frac{\partial V_0}{\partial X} \, \mathrm{d}X = \int_I \mathcal{G}_{\text{eff}}(\mathcal{E}_0) \frac{\partial \mathcal{E}_0}{\partial t} \, \mathrm{d}X. \tag{76}$$

Introducing the antiderivative $\mathcal{J}_{\text{eff}}$ of $\mathcal{G}_{\text{eff}}$ that vanishes when $\mathcal{E}_0 = 0$, i.e.

$$\mathcal{J}_{\text{eff}}(\mathcal{E}_0) = \int_0^{\mathcal{E}_0} \mathcal{G}_{\text{eff}}(\tilde{\mathcal{E}}_0) \, \mathrm{d}\tilde{\mathcal{E}}_0, \tag{77}$$

then (76) can be rewritten as

$$\int_I \mathcal{G}_{\text{eff}}(\mathcal{E}_0) \frac{\partial \mathcal{E}_0}{\partial t} \, \mathrm{d}X = \int_I \frac{\partial \mathcal{J}_{\text{eff}}(\mathcal{E}_0)}{\partial \mathcal{E}_0} \frac{\partial \mathcal{E}_0}{\partial t} \, \mathrm{d}X = \frac{\mathrm{d}}{\mathrm{d}t} \int_I \mathcal{J}_{\text{eff}}(\mathcal{E}_0) \, \mathrm{d}X. \tag{78}$$

Going back to (77), then making the substitution $\tilde{\Sigma}_0 = \mathcal{G}_{\text{eff}}(\tilde{\mathcal{E}}_0)$ and integrating by parts lead to

$$\begin{aligned} \mathcal{J}_{\text{eff}}(\mathcal{E}_0) &= \int_0^{\Sigma_0} \tilde{\Sigma}_0 \, (\mathcal{G}_{\text{eff}}^{-1})'(\tilde{\Sigma}_0) \, \mathrm{d}\tilde{\Sigma}_0, \\ &= \Sigma_0 \mathcal{E}_0 - \int_0^{\Sigma_0} \mathcal{G}_{\text{eff}}^{-1}(\tilde{\Sigma}_0) \, \mathrm{d}\tilde{\Sigma}_0, \end{aligned} \tag{79}$$

since Assumptions 2 imply that the effective strain-stress relation (32) satisfies $\mathcal{G}_{\text{eff}}(0) = 0$. Noticeably, the last identity in (79) amounts to the well known relation between the strain-based mechanical quantity $\mathcal{J}_{\text{eff}}(\mathcal{E}_0)$, which will be shown to be an energy, and the complementary stress-based one $\mathcal{J}^c_{\text{eff}}(\Sigma_0) = \int_0^{\Sigma_0} \mathcal{G}_{\text{eff}}^{-1}(\tilde{\Sigma}_0) \mathrm{d}\tilde{\Sigma}_0$. Such a relation can be established using the Legendre-Fenchel transform.

Making use of the explicit form (32) of $\mathcal{G}_{\text{eff}}^{-1}$ in (79) entails

$$\begin{aligned} \mathcal{J}_{\text{eff}}(\mathcal{E}_0) &= \frac{1}{2} \left\langle \frac{1}{E} \right\rangle \Sigma_0^2 + \frac{\Sigma_0}{h} \mathcal{R}^{-1}\left(\frac{1}{K} \Sigma_0 \right) - \int_0^{\Sigma_0} \frac{1}{h} \mathcal{R}^{-1}\left(\frac{1}{K} \tilde{\Sigma}_0 \right) \mathrm{d}\tilde{\Sigma}_0, \\ &= \frac{1}{2} \left\langle \frac{1}{E} \right\rangle \Sigma_0^2 + \int_0^{\Sigma_0} \frac{\tilde{\Sigma}_0}{Kh} (\mathcal{R}^{-1})'\left(\frac{1}{K} \tilde{\Sigma}_0 \right) \mathrm{d}\tilde{\Sigma}_0. \end{aligned} \tag{80}$$

In the integrated term of the equation above, making the substitution $\tilde{\Sigma}_0 = K\mathcal{R}(\zeta)$ gives

$$\int_0^{\Sigma_0} \frac{\tilde{\Sigma}_0}{Kh}(\mathcal{R}^{-1})'\left(\frac{1}{K}\tilde{\Sigma}_0\right) \mathrm{d}\tilde{\Sigma}_0 = \frac{K}{h}\int_0^{\mathcal{R}^{-1}(\Sigma_0/K)} \mathcal{R}(\zeta)\,\mathrm{d}\zeta. \tag{81}$$

Finally, using (81) in (80) and substituting back in (78) and (75) lead to

$$\frac{\mathrm{d}}{\mathrm{d}t}\int_I \left\{\frac{1}{2}\langle\rho\rangle V_0^2 + \frac{1}{2}\left\langle\frac{1}{E}\right\rangle \Sigma_0^2 + \frac{1}{2h}MV_0^2 + \frac{K}{h}\int_0^{\mathcal{R}^{-1}(\Sigma_0/K)} \mathcal{R}(\zeta)\,\mathrm{d}\zeta\right\}\mathrm{d}X$$
$$- \Big[\Sigma_0(\cdot,t)V_0(\cdot,t)\Big]_a^b = \int_I FV_0\,\mathrm{d}X$$

Making use of the notation of (38) and setting $C_0(t) = -\big[\Sigma_0(\cdot,t)V_0(\cdot,t)\big]_a^b$, then the previous equation can be rewritten as

$$\frac{\mathrm{d}}{\mathrm{d}t}(\mathscr{E}_0^m + \mathscr{E}_0^i) + C_0(t) = \int_I FV_0\,\mathrm{d}X$$

To conclude, we also have that $\mathscr{E}_0^m(t) \geq 0$ holds for all time $t \geq 0$, as well as $\mathscr{E}_0^i(t) \geq 0$ since the integral (81) is positive based on (74). Moreover, if $(\mathscr{E}_0^m + \mathscr{E}_0^i) = 0$ then the fields V_0 and Σ_0, which are continuous, vanish in the interval I, and so does $\mathcal{E}_0$.

C Proof of Property 5

We need to start by remarking that, using integration by part, we have

$$\mathcal{A} = 1 - \langle\alpha y\rangle, \qquad \mathcal{B} = 1 - \left\langle\frac{y}{\beta}\right\rangle, \qquad \left\langle\frac{a}{\beta}\right\rangle = 1 - \langle\alpha b\rangle. \tag{82}$$

We can hence rewrite (54) as

$$s(u_0) = \frac{\partial}{\partial x}\left(\mathcal{C}_1\frac{\partial^2 u_0}{\partial\tau^2}\right) + \mathcal{C}_2\frac{\partial^3 u_0}{\partial x\partial\tau^2} + \mathcal{C}\frac{\partial^2\sigma_0}{\partial\tau^2}, \tag{83}$$

where, making use of Property 4, we have

$$\mathcal{C}_1(x,\tau) = g'_{\mathrm{eff}}(\varepsilon_0)\{(m+1)d_1(\varepsilon_0) - d_0(\varepsilon_0)\}, \qquad \mathcal{C}_2 = -\frac{m}{2}, \qquad \mathcal{C} = \mathcal{B} - \langle\alpha b\rangle + m\left(\mathcal{B} - \frac{1}{2}\right).$$

By definition (24) of σ_0 and two successive applications of the chain rule, remembering that $\varepsilon_0 = \partial u_0/\partial x$, we find that

$$\begin{aligned}\frac{\partial^2\sigma_0}{\partial\tau^2} &= g'_{\mathrm{eff}}(\varepsilon_0)\frac{\partial^3 u_0}{\partial x\partial\tau^2} + g''_{\mathrm{eff}}(\varepsilon_0)\left(\frac{\partial^2 u_0}{\partial x\partial\tau}\right)^2,\\ &= \frac{\partial}{\partial x}\left(g'_{\mathrm{eff}}(\varepsilon_0)\frac{\partial^2 u_0}{\partial\tau^2}\right) - \frac{\partial}{\partial x}(g'_{\mathrm{eff}}(\varepsilon_0))\frac{\partial^2 u_0}{\partial\tau^2} + g''_{\mathrm{eff}}(\varepsilon_0)\left(\frac{\partial^2 u_0}{\partial x\partial\tau}\right)^2.\end{aligned} \tag{84}$$

Moreover, using (84) and the fact that $\mathcal{C}_2$ and $\mathcal{C}$ are constants, then (83) can be rewritten as

$$s(u_0) = \frac{\partial}{\partial x}\left((\mathcal{C}_1 + \mathcal{C}_2 + \mathcal{C}g'_{\mathrm{eff}}(\varepsilon_0))\frac{\partial^2 u_0}{\partial\tau^2}\right) - \mathcal{C}\frac{\partial}{\partial x}(g'_{\mathrm{eff}}(\varepsilon_0))\frac{\partial^2 u_0}{\partial\tau^2} + \mathcal{C}g''_{\mathrm{eff}}(\varepsilon_0)\left(\frac{\partial^2 u_0}{\partial x\partial\tau}\right)^2. \tag{85}$$

Now, it is remarkable that, using (82) and a little algebra, we can show that

$$\mathcal{C}_1 + \mathcal{C}_2 + \mathcal{C}g'_{\mathrm{eff}}(\varepsilon_0) = 0. \tag{86}$$

Finally, remembering that $\varepsilon_0 = \partial u_0/\partial x$, we have by direct differentiation that $\frac{\partial}{\partial x}(g'_{\text{eff}}(\varepsilon_0)) = \frac{\partial^2 u_0}{\partial x^2} g''_{\text{eff}}(\varepsilon_0)$, which, used together with (86) allows us to rewrite (85) as

$$s(u_0) = \mathcal{C} g''_{\text{eff}}(\varepsilon_0) \left\{ \left(\frac{\partial^2 u_0}{\partial x \partial \tau} \right)^2 - \frac{\partial^2 u_0}{\partial x^2} \frac{\partial^2 u_0}{\partial \tau^2} \right\},$$

as expected.

Simplifications can occur in two particular cases. Firstly, in the case of a homogeneous material (without restriction on the linearity or non-linearity of the imperfect interface), we have that $\beta(y) = \alpha(y) = 1$, implying that $\langle \alpha b \rangle = \mathcal{B}$, $b(y) = y$ and $\mathcal{B} = 1/2$, resulting in $\mathcal{C} = 0$. Hence for a homogeneous material, such as that dealt with in Section 5.3, the source term $s(u_0)$ is identically zero.

Secondly, using again the differentiation formulae for inverse functions, we can show that

$$g''_{\text{eff}}(\varepsilon_0) = \frac{h}{\mathscr{k}^2} \left(\frac{g'_{\text{eff}}(\varepsilon_0)}{\phi(\varepsilon_0)} \right)^3 \mathcal{R}''(h \, [\![u_1(x, \cdot, \tau)]\!]). \tag{87}$$

In the linear case, where $\mathcal{R}(\zeta) = \zeta$ and $\mathcal{R}'' = 0$, we therefore have $g''_{\text{eff}}(\varepsilon_0) = 0$, and (87) implies that, for an arbitrary medium, but with linear imperfect interfaces, we can also conclude that the source term $s(u_0)$ is identically zero.

Acknowledgment: All authors are grateful to the Royal Society for financial support via the International Exchange grant IEC/R2/170087.

References

[1] A. Abdulle and P. Henning. Chapter 20 - Multiscale Methods for Wave Problems in Heterogeneous Media. In Rémi Abgrall and Chi-Wang Shu, editors, *Handbook of Numerical Methods for Hyperbolic Problems*, volume 18 of *Handbook of Numerical Analysis*, pages 545 – 576. Elsevier, 2017.

[2] J. D. Achenbach and A. N. Norris. Loss of specular reflection due to nonlinear crack-face interaction. *Journal of Nondestructive Evaluation*, 3(4):229–239, 1982.

[3] I.V. Andrianov, V.V. Danishevs'kyy, H. Topol, and D. Weichert. Homogenization of a 1D nonlinear dynamical problem for periodic composites. *ZAMM - Journal of Applied Mathematics and Mechanics / Zeitschrift für Angewandte Mathematik und Mechanik*, 91(6):523–534, 2011.

[4] Y. C. Angel and J. D. Achenbach. Reflection of ultrasonic waves by an array of microcracks. In D.O. Thompson and D.E. Chimenti, editors, *Review of Progress in Quantitative Nondestructive Evaluation*, pages 83–89. Springer, 1985.

[5] Raphaël C. Assier, Marie Touboul, Bruno Lombard, and Cédric Bellis. High-frequency homogenization in periodic media with imperfect interfaces. *Proceedings of the Royal Society A: Mathematical, Physical and Engineering Sciences*, 476(2244):20200402, 2020.

[6] J.-M. Baik and R. B. Thompson. Ultrasonic scattering from imperfect interfaces: A quasi-static model. *J. Nondestruct. Eval.*, 4(3-4):177–196, 1984.

[7] S.C. Bandis, A.C. Lumsden, and N.R. Barton. Fundamentals of rock joint deformation. *International Journal of Rock Mechanics and Mining Sciences & Geomechanics Abstracts*, 20(6):249 – 268, 1983.

[8] A. Bensoussan, J.-L. Lions, and G. Papanicolaou. *Asymptotic analysis for periodic structures*. AMS Chelsea Publishing, 2011.

[9] D. Broda, W.J. Staszewski, A. Martowicz, T. Uhl, and V.V. Silberschmidt. Modelling of nonlinear crack–wave interactions for damage detection based on ultrasound—a review. *Journal of Sound and Vibration*, 333(4):1097 – 1118, 2014.

[10] R. Cornaggia and B. B. Guzina. Second-order homogenization of boundary and transmission conditions for one-dimensional waves in periodic media. *International Journal of Solids and Structures*, 188-189:88 – 102, 2020.

[11] R. Cornaggia and B. Lombard. *Transient waves in 1D periodic media : second-order homogenization of transmission conditions and source points*. In preparation.

[12] C. D. Dafermos. *Hyperbolic Conservation Laws in Continuum Physics*. Springer, 2005.

[13] E. Godlewski and P.A. Raviart. *Numerical Approximation of Hyperbolic Systems of Conservation Laws*. Springer, 1996.

[14] V. Gusev, B. Castagnède, and A. Moussatov. Hysteresis in response of nonlinear bistable interface to continuously varying acoustic loading. *Ultrasonics*, 41(8):643 – 654, 2003.

[15] Z. Hashin. Thermoelastic properties of fiber composites with imperfect interface. *Mechanics of Materials*, 8:333–348, 1990.

[16] Z. Hashin. Thin interphase/imperfect interface in elasticity with application to coated fiber composites. *J. Mech. Phys. Solids*, 50(12):2509–2537, 2002.

[17] K. L. Johnson. *Contact Mechanics*. Cambridge University Press, 1985.

[18] S. Junca and B. Lombard. Dilatation of a one-dimensional nonlinear crack impacted by a periodic elastic wave. *SIAM Journal on Applied Mathematics*, 70(3):735–761, 2009.

[19] S. Junca and B. Lombard. Dilatation of a one-dimensional nonlinear crack impacted by a periodic elastic wave. *SIAM Journal on Applied Mathematics*, 70(3):735–761, 2009.

[20] S. Junca and B. Lombard. Interaction between periodic elastic waves and two contact nonlinearities. *Mathematical Models and Methods in Applied Sciences*, 22(04):1150022, 2012.

[21] J. Kevorkian and D. L. Bosley. Multiple-scale homogenization for weakly nonlinear conservation laws with rapid spatial fluctuations. *Studies in Applied Mathematics*, 101(2):127–183, 1998.

[22] A. Lamacz. Dispersive effective models for waves in heterogeneous media. *Mathematical Models and Methods in Applied Sciences*, 21(09):1871–1899, 2011.

[23] P. D. Lax. Hyperbolic systems of conservation laws ii. *Comm. Pure Appl. Math.*, 10(4):537–566, 1957.

[24] P. D. Lax. Development of singularities of solutions of nonlinear hyperbolic partial differential equations. *J. Math. Phys.*, 5(5):611–613, 1964.

[25] F. Lebon and R. Rizzoni. Asymptotic behavior of a hard thin linear elastic interphase: An energy approach. *International Journal of Solids and Structures*, 48(3):441 – 449, 2011.

[26] F. Lebon and R. Rizzoni. Higher order interfacial effects for elastic waves in one dimensional phononic crystals via the Lagrange-Hamilton's principle. *European Journal of Mechanics - A/Solids*, 67:58 – 70, 2018.

[27] R.J. LeVeque. *Finite Volume Methods for Hyperbolic Problems*. Cambridge Texts in Applied Mathematics, 2002.

[28] C. Licht, F. Lebon, and A. Léger. Dynamics of elastic bodies connected by a thin adhesive layer. In A. Leger and M. Deschamps, editors, *Ultrasonic Wave Propagation in Non Homogeneous Media*, volume 128, pages 99–110. Springer Proceedings in Physics, 2009.

[29] B. Lombard. Modélisation numérique de la propagation et de la diffraction d'ondes mécaniques. Habilitation Thesis, Université d'Aix-Marseille 2, 2010.

[30] B. Lombard and J. Piraux. How to incorporate the spring-mass conditions in finite-difference schemes. *SIAM J. Sci. Comput.*, 24(4):1379–1407, 2003.

[31] B. Lombard and J. Piraux. Modeling 1-D elastic P-waves in a fractured rock with hyperbolic jump conditions. *J. Comput. App. Math.*, 204:292–305, 2007.

[32] J. C. López-Realpozo, R. Rodríguez-Ramos, R. Guinovart-Díaz, J. Bravo-Castillero, L. Pérez Fernández, F. J. Sabina, and G. A. Maugin. Effective properties of non-linear elastic laminated composites with perfect and imperfect contact conditions. *Mech. Adv. Mater. Struc.*, 15(5):375–385, 2008.

[33] S. Nakagawa, K.T. Nihei, and L.R. Myer. Stop-pass behavior of acoustic waves in a 1D fractured system. *J. Acoust. Soc. Am.*, 107-1:40–50, 2000.

[34] H. Nassar, Q.-C. He, and N. Auffray. Willis elastodynamic homogenization theory revisited for periodic media. *Journal of the Mechanics and Physics of Solids*, 77:158 – 178, 2015.

[35] C. Pecorari. Nonlinear interaction of plane ultrasonic waves with an interface between rough surfaces in contact. *The Journal of the Acoustical Society of America*, 113(6):3065–3072, 2003.

[36] L.J. Pyrak-Nolte, L.R. Myer, and N.G.W. Cook. Anisotropy in seismic velocities and amplitudes from multiple parallel fractures. *J. Geophys. Res.*, 95-7:345–358, 1990.

[37] J. M. Richardson. Harmonic generation at an unbonded interface—i. planar interface between semi-infinite elastic media. *International Journal of Engineering Science*, 17(1):73 – 85, 1979.

[38] S. I. Rokhlin and Y. J. Wang. Analysis of boundary conditions for elastic wave interaction with an interface between two solids. *J. Acoust. Soc. Am.*, 89(2):503–515, 1991.

[39] E Sanchez-Palencia. *Non-Homogeneous Media and Vibration Theory*. Springer, Berlin, Heidelberg, 1978.

[40] F. Santosa and W. W. Symes. A dispersive effective medium for wave propagation in periodic composites. *SIAM Journal on Applied Mathematics*, 51(4):984–1005, 1991.

[41] M. Schoenberg. Elastic wave behavior across linear slip interfaces. *J. Acoust. Soc. Am.*, 68(5):1516–1521, 1980.

[42] I. Sevostianov, R. Rodriguez-Ramos, R. Guinovart-Diaz, J. Bravo-Castillero, and F.J. Sabina. Connections between different models describing imperfect interfaces in periodic fiber-reinforced composites. *International Journal of Solids and Structures*, 49(13):1518 – 1525, 2012.

[43] I. Y. Solodov. Ultrasonics of non-linear contacts: propagation, reflection and NDE-applications. *Ultrasonics*, 36(1):383 – 390, 1998.

[44] J. R. Willis. Effective constitutive relations for waves in composites and metamaterials. *Proceedings of the Royal Society A: Mathematical, Physical and Engineering Sciences*, 467(2131):1865–1879, 2011.

[45] J.R. Willis. Variational principles for dynamic problems for inhomogeneous elastic media. *Wave Motion*, 3(1):1 – 11, 1981.